The Emission, Transport, and Impacts of the Extreme Saharan Dust Storm in 2015

Brian Harr, Bing Pu, Qinjian Jin

Department of Geography and Atmospheric Science, University of Kansas, Lawrence, KS, 66045, United States

5   *Correspondence to*: Brian Harr (bharr125@ku.edu), Bing Pu (bpu@ku.edu)

Abstract. Each summer, the Saharan Air Layer transports massive amounts of mineral dust across the Atlantic Ocean, affecting weather, climate, and public health over large areas. Despite the considerable impacts of African dust, the causes and impacts of extreme trans-Atlantic African dust events are not fully understood. The "Godzilla" trans-Atlantic dust event in 2020 has been extensively studied, but little is known about other similar events. Here we examine the June 2015 event, the second

10   strongest trans-Atlantic African dust event during summers over 2003–2022. This event was characterized by moderately high dust emissions over western North Africa and an extremely high aerosol optical depth (AOD) over the tropical North Atlantic. The high dust loading over the Atlantic is associated with atmospheric circulation extremes like the "Godzilla" event. Both the African easterly jet (AEJ) and Caribbean low-level jet (CLLJ) are greatly intensified, along with a westward extension of the North Atlantic subtropical high (NASH), all of which favor the westward transport of African dust. The enhanced dust

15   emissions are related to anomalously strong surface winds in dust source regions and reduced vegetation density and soil moisture over the northern Sahel.

The dust plume reduced surface net shortwave radiation over the eastern tropical North Atlantic by about 25 W m^{-2} but increased net longwave flux by about 3 W m^{-2}. In contrast to the "Godzilla" event, the 2015 event had minor air quality impacts

20   on the U.S., partially due to the extremely intensified CLLJ that dispersed the dust plume to the Pacific.

1 Introduction

North Africa is the world's largest source of dust, emitting about 400 – 2200 Tg of mineral dust each year (e.g., Goudie and Middleton 2001; Huneeus et al. 2011; Wu et al. 2020; Kok et al. 2021). African dust aerosols can affect the Earth's radiation budget (Prospero and Lamb 2003; Li et al. 2004; Engelstaedter et al. 2006; Schepanski 2018; Francis et al. 2022), modify

25   cloud properties by serving as cloud condensation nuclei and ice nuclei (Levin et al. 1996; Rosenfeld et al. 2001; Goudie and Middleton 2001; Yin et al. 2002; DeMott et al. 2003; Prenni et al. 2009), and couple with global biogeochemical cycles when depositing vital mineral nutrients over land and ocean (Okin et al. 2004; Bristow et al. 2010; Kumar et al. 2014; Yu et al.

2015a; Jickells et al. 1998, 2016; Villar-Argaiz et al. 2018; Evans et al. 2019; Li et al. 2021b; Barkley et al. 2022). Climate change is expected to have major impacts on North Africa (Prospero et al. 2021), making it more pressing to understand the spatiotemporal variability of African dust and its associated impacts.

Each boreal summer a large amount of African dust is transported westward to the Atlantic Ocean. The thick, warm, and dry African dust plumes, namely the Saharan Air Layer (SAL; Carlson and Prospero 1972; Prospero and Carlson 1972; Karyampudi and Carlson 1988; Kanitz et al. 2014), can often propagate across the tropical North Atlantic to the Caribbean Basin and southeastern U.S., affecting weather and climate systems along their transport pathways (Karyampudi and Carlson 1988; Dunion and Velden 2004; Jenkins et al. 2008; Jenkins and Pratt 2008; Strong et al. 2018). While much of the research seeks to understand the conditions associated with African dust emissions and westward transport and to quantitatively characterize the trans-Atlantic African dust plumes (Prospero and Lamb 2003; Li et al. 2004; Kaufman et al. 2005; Engelstaedter et al. 2006; Kalashnikova and Kahn 2008; Peyridieu et al. 2010; Knippertz and Todd 2012; Evan et al. 2015; Fiedler et al. 2015; Yu et al. 2015b, 2019), only a small body of research is dedicated to examine the summertime extreme trans-Atlantic dust events, i.e., events with extremely high dust loading over the tropical North Atlantic (Huang et al. 2010; Francis et al. 2020; Yu et al. 2021; Pu and Jin 2021). The record-breaking trans-Atlantic African dust event in June 2020, namely, the "Godzilla" dust storm, is the strongest trans-Atlantic dust event in summer since 2003 (Yu et al. 2021; Pu and Jin 2021) and has been extensively studied (Francis et al. 2020; Yu et al. 2021; Pu and Jin 2021; Francis et al. 2022; Scott et al. 2022; Asutosh et al. 2022; Mehra et al. 2023). It is found that the event is associated with both enhanced dust emissions over North Africa and intensified westward transport of dust related to circulation extremes (Yu et al. 2021; Pu and Jin 2021). However, little is known about other similar extreme trans-Atlantic African dust events in summer. It is not clear what the major causes of the extremely high loading of African dust over the tropical North Atlantic are, e.g., whether mechanisms found in the 2020 event also apply to other events, and whether they resulted in similar radiation and air quality impacts.

To address some of these questions, we examine the June 2015 trans-Atlantic African dust storm, which is the second strongest aerosol extreme event over the tropical North Atlantic in boreal summer during 2003–2020 (Pu and Jin 2021), to better understand the formation and impacts of extreme trans-Atlantic dust events. We examine the characteristics, mechanism, and radiative and air quality impacts of this event using multiple satellite products, ground observations, and reanalysis data. The following section reviews previous studies of summertime trans-Atlantic African dust events. Section 3 introduces the data and methodology used in this study, while section 4 presents a detailed analysis of the June 2015 event and compares it with the 2020 "Godzilla" dust event. Section 5 discusses limitations and uncertainties, and section 6 summarizes our major findings.

2 Background

During summertime, strong surface heating in the Sahara initiates dry convection (Fontaine et al. 2002) carrying dust high into the atmosphere where it forms a deep, dry, well-mixed dust layer, i.e., the SAL (Carlson and Prospero 1972; Prospero et al.

2002; Barkan et al. 2004; Braun 2010; Pan et al. 2011; Dunion 2011; Adams et al. 2012). The SAL is bounded by two inversions vertically because the layer is often warmer than the surrounding environment at its base but cooler than normal tropical air at the top (Carlson and Prospero 1972; Braun 2010). The top layer of a SAL can reach 5~6 km while its base is often about 0.9~1.8 km above the surface (e.g., Prospero and Carlson 1972; Dunion and Velden 2004; Adams et al. 2012).

65 Early observational studies documented that SALs move westward from North Africa to the Caribbean, especially Barbados (Prospero and Carlson 1970; Prospero et al. 1970). It is estimated that least 72 Tg a^{-1} of African dust leaves the African west coast at 15°W in summer and about 18 Tg a^{-1} reaches 75°W in the Caribbean (Yu et al. 2015). The westward transport of the SAL in boreal summer has long been related to meteorological factors, such as the African easterly jet (AEJ) and African easterly wave (AEW) (Burpee 1972; Fontaine et al. 2002; Jones et al. 2003; Engelstaedter and Washington 2007).

70

Many other factors that either influence dust emissions in North Africa or affect atmospheric circulation over the tropical North Atlantic have been related to the summertime westward transport of African dust. For instance, Prospero and Lamb (2003) found that the concentrations of transported African dust in Barbados from 1965 to 1998 are positively related to prior year El Niño Southern Oscillation (ENSO) events. Specifically, El Niño events frequently result in dry conditions in Sudano-Sahel, leading to increased dust emissions. Recently, Li et al. (2021a) found that the Southern Oscillation index (negative in El Niño events) is positively correlated with MERRA-2 surface dust concentrations in North Africa during 1982-2019, with La Niña events corresponding to higher surface dust concentrations in North Africa. On the other hand, Yin et al. (2022) found no statistically significant correlations between ENSO and MERRA-2 dust column mass density in Saharan Africa during 1980-2021. These findings suggest that the connections between ENSO events and the emission and westward transport of African dust may be sensitive to study regions, dust variables, and time periods. In addition, the North Atlantic subtropical high (NASH; Doherty et al. 2008; Chen et al. 2018), the North Atlantic Oscillation (NAO; Moulin et al. 1997), drought and vegetation coverage in the Sahel (Moulin and Chiapello 2004; Yu et al. 2015b), and multi-decadal variability in Atlantic sea surface temperature (Wang et al. 2012) have also been related to the westward transport of African dust over the tropical North Atlantic.

85

While the above studies extensively examined the features and propagations of the SALs in summer, only a few studies focused on extreme trans-Atlantic dust African events that lead to high dust loading over the tropical North Atlantic and the Caribbean Basin. For instance, Petit et al. (2005) examined the extreme trans-Atlantic dust event in June 1994. The dust plume originated near the saltpan of Taoudenni in northern Mali, where strong surface winds and convection associated with a depression lifted

90 dust to about 5 km. The dust plume then gradually descended as it traversed the Atlantic within the easterly trades to Guadeloupe. The peak Infrared Difference Dust Index reached 18 K (corresponding to an aerosol optical depth of about 1.5~4.5) over Taoudenni. The plume led to a visibility reduction from 25–30 km to 9 km in Guadeloupe. They also noticed that the transport of Saharan dust to the Caribbean was always connected with the propagation of the SAL, but the SAL did not always contain a dust plume.

95

The summer of 2006 had several significant Saharan dust events. Bou Karam et al. (2014) examined an event on 3-5 August 2006. This event was initiated by a cold pool outflow from a mesoscale convective system (MCS) over western North Africa. The dust plume was then exported by the AEJ towards the Caribbean. Knippertz and Todd (2010) examined the same event and three others, one on 17-18 July, and two more in September, and how these events related to AEW cyclonic flows. The

100 above studies mainly focused on the formation of extreme dust plumes over the Sahara but did not examine the westward propagation of the extreme dust plumes across the tropical North Atlantic.

Huang et al. (2010) conducted a comprehensive study of major trans-Atlantic African dust outbreaks from 2003 to 2007. Dust outbreaks were defined when regionally averaged daily MODIS aerosol optical depth (AOD) exceeded the climatological

105 mean by one standard deviation over the eastern tropical North Atlantic between 0–30°N and 15–25°W. Their findings, based on satellite products and reanalysis data, painted a detailed picture of dust transport from central Western Africa to the Caribbean Basin, documenting the westward transport pathways of dust, the speed and altitude of dust layers, and their connection with dry air outbreaks. While Huang et al. (2010) are among the first to systemically study severe trans-Atlantic dust outbreaks, they did not examine the large-scale circulation conditions supporting dust long-range transport, nor the local

110 land surface conditions associated with dust emissions.

The formation of the recent extreme trans-Atlantic Saharan dust event in June 2020 has been related to both enhanced local emissions associated with increased surface winds, reduced vegetation coverage (Pu and Jin 2021), and intense cold pool outflows from strong haboobs (Yu et al. 2021) and large-scale circulations that favored the westward transport of African dust

115 (Francis et al. 2020; Yu et al. 2021; Pu and Jin 2021). Pu and Jin (2021) pointed out that atmospheric circulation extremes played critical roles in this event. The extremely enhanced AEJ (the strongest for the weeks of June 14–27 in 1979-2020) advected huge amounts of dust to the eastern tropical North Atlantic. The westward extension of the NASH over the western tropical Atlantic and the greatly intensified CLLJ (the second strongest for the week of June 21–27 during 1979–2020) over the Caribbean Basin further steered the dust plume westward and northward to the U.S. We will examine whether similar

120 atmospheric circulation patterns and land surface conditions occurred in the June 2015 event and if circulation extremes also contributed to the high dust loading over the Atlantic.

Dust aerosols can absorb and scatter incoming shortwave and outgoing longwave radiation and also emit longwave radiation, affecting the regional and global radiative balance (Claquin et al. 2003; Xu et al. 2017). The sign and magnitude of the radiative

125 forcing of dust strongly depend on dust particle size and shape, horizontal and vertical distributions of dust aerosols, and their chemical and mineral compositions (Goudie and Middleton 2001; Meloni et al. 2005; Reddy et al. 2013; Mahowald et al. 2014; Kok et al. 2023), the direct observations of which are still lacking at large scales. The radiative effects of African dust have long been examined through satellite products (e.g., Yu et al. 2006; Brindley and Russell 2009; Song et al. 2018), field campaigns with surface and aircraft measurements (e.g., Carlson and Caverly 1977; Haywood et al. 2001, 2003; Highwood et

130 al. 2003; Slingo et al. 2006), and modelling studies (e.g., Tegen and Lacis 1996; Myhre et al. 2003; Tegen et al. 2010; Hansell

et al. 2010). While the longwave effect of dust aerosols at the top of the atmosphere (TOA) is generally a warming effect, the shortwave effect depends on surface albedo; and the net effect is the balance of the two and is estimated to be -0.48 ~ 0.20 Wm^{-2} globally (Kok et al. 2017). The high dust loading and long duration of extreme trans-Atlantic dust events provide great examples to understand the radiative impacts of African dust. Francis et al. (2022) examined the radiative effect of the

135   "Godzilla" dust plume in 2020 and found up to a 190 W m^{-2} drop in downward shortwave radiation flux and a 23 W m^{-2} rise in downward longwave flux at the surface over the eastern tropical Atlantic on June 18. Mehra et al. (2023) found that the "Godzilla" dust plume also impacted radiative balance in the U.S., resulting in atmospheric heating of 5~12 W m^{-2}. Here we will explore the perturbation of the June 2015 African dust plume on both surface and TOA radiative budgets.

140   Severe dust storms with elevated concentrations of dust particles can have adverse impacts on public health and transportation (Shinn et al. 2003; Goudie 2014; Española et al. 2021). Trans-Atlantic African dust is found to affect air quality over both the Caribbean Basin and the southern U.S. (Prospero 1999; Chen et al. 2018; Prospero et al. 2021). For instance, Saharan dust is found to be related to high rates of asthma in the Caribbean (Gyan et al. 2005; Akpinar-Elci et al. 2015) and serves as a carrier for fungi and bacteria from Africa to the Caribbean (Prospero et al. 2005; Waters et al. 2020). Over coastal Texas, African

145   dust contributed approximately 8% of PM$_{2.5}$ (particulate matter with aerodynamic diameter < 2.5 µm) concentrations during summertime, and up to 48% of PM$_{2.5}$ during an African dust outbreak in August 2014 (Bozlaker et al. 2019). During the "Godzilla" event in 2020, PM$_{2.5}$ levels over a large area of the southern U.S. exceeded the Environmental Protection Agency (EPA)'s guideline, and the Air Quality Index (AQI) reached orange (unhealthy for sensitive groups) and red (unhealthy for the general public) levels in more than 11 states (Pu and Jin 2021; Yu et al. 2021). To what extent the 2015 extreme trans-Atlantic

150   dust affected the air quality in the U.S. will be examined in this study.

3 Data and Methodology

3.1 Data

We use satellite retrievals of AOD, radiative fluxes, vegetation coverage, and precipitation, as well as circulation variables and soil moisture from reanalysis and ground observations of AOD and air quality variables to examine the characteristics,

155   mechanisms, and impacts of the 2015 extreme dust plume.

3.1.1 MODIS and VIIRS AOD

AOD is a column-integrated measure of aerosol extinction. Here, daily and monthly AOD from the Moderate Resolution Imaging Spectroradiometer (MODIS) (version 6.1; Sayer et al. 2019) aboard both the Terra and Aqua satellites are used. Monthly level 3 AOD data from 2003 to 2022 have a spatial resolution of 1.0° × 1.0°, while daily level 2 data in 2015 are re-

160   gridded to a 0.1° × 0.1° grid to characterize features of the dust plume. Monthly and daily MODIS AOD is generated by averaging Terra and Aqua MODIS AOD.

Daily AOD from the Visible Infrared Imaging Radiometer Suite (Hsu et al. 2019) on board the Suomi National Polar-Orbiting Partnership (Suomi-NPP) satellite is used to complement MODIS AOD. Daily VIIRS AOD is also gridded to a 0.1° × 0.1°

165   resolution and averaged with MODIS AOD during June 2015 to increase data spatial coverage to better demonstrate the propagation of the African dust plume. Both MODIS and VIIRS AOD agree well with the Aerosol Robotic Network (AERONET; Holben et al. 1998, 2001) ground observations (Liu et al. 2014; Sayer et al. 2019; Hsu et al. 2019), with root mean square errors of 0.115, 0.121 and 0.122 for Aqua-MODIS, Terra-MODIS, and VIIRS, respectively (Hsu et al. 2019).

3.1.2 CALIOP Aerosol Profiles

170   The Cloud-Aerosol Lidar with Orthogonal Polarization (CALIOP) is a two-wavelength lidar instrument aboard the Cloud-Aerosol Lidar and Infrared Pathfinder Satellite Observations (CALIPSO) satellite. CALIOP measures backscattered radiances attenuated by aerosols and clouds and retrieves the microphysical and optical properties of aerosols. The record began in June 2006 and has been shown to provide quality data about aerosol size, type, and different shapes of cloud particles (Winker et al. 2007). We use daily 532 nm total attenuated backscatter (level 1) and depolarization ratio (δ; level 2) in June 2015 to

175   examine the vertical profiles of the dust plume. Note that CALIOP data are missing from 19–28 June 2015. Since the depolarization ratio can help separate spherical and non-spherical hydrometeors (Sassen 1991), we use $\delta \geq 0.2$ to separate dust (non-spherical) from other aerosols (Li et al. 2010; Kim et al. 2018; Pu and Ginoux 2018a; Pu and Jin 2021).

3.1.3 SEVIRI dust RGB

Dust red-green-blue (RGB) composite satellite images have been widely used as a qualitative method to study the

180   spatiotemporal formation and evolution of dust plumes (e.g., Schepanski et al. 2007; Marsham et al. 2008; Martínez et al. 2009; Roberts et al. 2018; Caton Harrison et al. 2021). Dust aerosols are detected based on spectral varying emissivity at the infrared (IR) wavelengths ranging from 8 to 12 μm (Ackerman 1997; Lensky and Rosenfeld 2008). Here, the dust RGB images from the Spinning Enhanced Visible and Infrared Imager (SEVIRI) onboard the geostationary Meteosat Second Generation (MSG) satellite (Schmetz et al. 2002) positioned at 0° longitude (i.e., Meteosat-10) are used to understand dust emissions

185   during the June 2015 extreme event. SEVIRI observes the Earth system at 12 wavelengths ranging from 0.4 to 13.4 μm with a 15-minute repeat cycle and a spatial resolution of 3 km at nadir for the IR channels. SEVIRI dust RGB images are composed of brightness temperatures (BT) and BT difference (BTD) at 8.7, 10.8, and 12.0 μm (Schepanski et al. 2007; Ashpole and Washington 2012). The dust RGB bands are defined as follows: BTD of 12.0−10.8 μm is red, BTD of 10.8−8.7 μm is green, and BT at 10.8 μm is blue. The dust plumes appear as magenta in the dust RGB images. IR dust detection is affected by several

190   factors, such as, the vertical temperature gradient in the lower atmosphere, water vapor content, dust mineralogy, dust altitudes, and characteristics of the land surface (Brindley et al. 2012).

3.1.4 MODIS NDVI

We also use monthly and 16-day MODIS Normalized Difference Vegetation Index (NDVI; Didan et al. 2015) to examine the connection between dust emissions and vegetation coverage. The level 3 data are interpolated to a 0.25° × 0.25° grid, and the
195   16-day products are linearly interpolated to daily values.

3.1.5 IMERG

The Global Precipitation Measurement Mission (GPM) utilizes the Integrated Multi-Satellite Retrievals for GPM (IMERG) algorithm to combine all available low-Earth-orbit and geosynchronous-Earth-orbit satellite passive microwave (PMW) and infrared (IR) precipitation estimates and is then validated and bias-corrected with monthly gauge analysis from the Global
200   Precipitation Climatology Centre (GPCC) (Huffman et al. 2018). IMERG is an improvement over the previous Tropical Rainfall Measuring Mission (TRMM), with reduced miss-detection of precipitation and better performance in capturing heavy and light precipitation (Wang et al. 2021) and sub-daily rainfall (Freitas et al. 2020), but still has large overestimations of duration and underestimations of intensity of precipitation (Freitas et al. 2020). We use IMERG Final Run (IMERG-F) from 2000 to 2019 (0.1° by 0.1°) as it is the most accurate, gauge-adjusted, and research-ready IMERG product (Wang et al. 2017,
205   2021; Beck et al. 2021). The half-hourly data are resampled to daily averages to examine the potential influence of precipitation on the formation and transport of the extreme African dust plume.

3.1.6 CERES Radiative Fluxes

We use daily and monthly radiation flux data from the Clouds and the Earth's Radiant Energy System (CERES) products (Doelling et al. 2016) on a 1°×1° grid to study the radiative impacts of the extreme 2015 dust plume. The CERES instruments
210   are onboard both the Terra and Aqua satellites, measuring shortwave (SW) radiation between 0.3 and 5 µm, total radiation between 0.3 and 200 µm, and window wavelengths between 8 and 12 µm (Wielicki et al. 1996). The dataset includes observed top of the atmosphere (TOA) fluxes and computed surface and in-atmosphere fluxes using Langley Fu-Liou radiative transfer model and MODIS and geostationary satellite-derived cloud properties, along with atmospheric data from GEOS-5.4.1 and aerosol prosperities from the Model for Atmospheric Transport and Chemistry (MATCH) that assimilates MODIS AOD
215   (Rutan et al. 2015). Note that current CERES products have a net imbalance of +4.5 W m^{-2} at TOA (Johnson et al. 2016; Kato et al. 2018; Loeb et al. 2018). In comparison with surface observations on buoy sites, CERES surface fluxes show mean biases of 3.0 W m^{-2} for downward SW and -4.0 W m^{-2} for downward longwave (LW) fluxes in monthly data. The larger differences between the CERES and buoy data over the tropical Atlantic Ocean are attributed to the transported African dust that

accumulated on buoys (Foltz et al. 2013). Due to its high spatial coverage, CERES products have been widely used to study
220 the radiative effect of dust (e.g., Song et al. 2018; Francis et al. 2022).

3.1.7 AERONET AOD

The AERONET program (Holben et al. 1998) provides quality-assured cloud-screened (level 2.0) measurements of aerosol
optical properties from sun photometer records. The recorded AOD has high accuracy with an uncertainty level of 0.01~0.02
(wavelength dependent) (Holben et al. 2001; Giles et al. 2019). Here version 3.0 AOD at wavelengths between 440 nm and
225 870 nm and Ångström exponents across the dual wavelength of 440–675, 440–870, and 500–870 nm with temporal resolutions
varying from about 3 to 30 minutes (station dependent) over western North Africa, the tropical North Atlantic, and Caribbean
Basin in June 2015 are used. AOD at 550 nm is converted using the method detailed by Pu et al. (2020). Stations with records
less than 10 days and AOD mean values over 11–25 June 2015 lower than 0.2 are not included in the analysis. The results of
14 stations are presented and compared with MODIS and VIIRS AOD.

230 ### 3.1.8 EPA Station Data

Daily air quality data of $PM_{2.5}$ and the Air Quality Index (AQI) from the U.S. Environmental Protection Agency's (EPA) Air
Quality System (AQS) stations are used to examine the influence of the June 2015 African dust plume on air quality in the
U.S. AQI reflects the health effect of major air pollutants, with values of 0–50 indicate good air quality (symbolized by green),
51–100 for moderate condition (yellow), 101–150 for unhealthy for sensitive groups (orange), and 151–200 for unhealthy
235 condition (red).

3.1.9 MERRA-2 Aerosol Products

The Modern-Era Retrospective analysis for Research and Applications, Version 2 (MERRA-2; Gelaro et al. 2017) provides a
dust optical depth (DOD) (~ 50 km; 3-hourly) beginning in 1980. MERRA-2 is the first long-term global reanalysis that
incorporates satellite observations of aerosols (Gelaro et al. 2017). MERRA-2 assimilates aerosol products from MODIS,
240 Multi-angle Imaging SpectroRadiometer (MISR), and Advanced Very-High-Resolution Radiometer (AVHRR) as well as
ground observations from AERONET sun photometers (Gelaro et al. 2017; Buchard et al. 2017). MERRA-2 shows
considerable skill in its aerosol products and improvement over its predecessor (Gelaro et al. 2017; Randles et al. 2017;
Buchard et al. 2017). Its DOD product well captures the spatial and temporal variations in DOD over North Africa on the
seasonal time scale in comparison with infrared satellite retrievals but misses a large part of day-night differences of dust as
245 night-time observations currently are not assimilated to the product (Tindan et al. 2023). The 3-hourly MERRA2- DOD are
averaged to daily data to complement MODIS and VIIRS AOD.

3.1.10 ERA5 Meteorological and Surface Variables

European Centre for Medium-range Weather Forecasts (ECMWF) Reanalysis 5 (ERA5) (Hersbach et al. 2020; Muñoz-Sabater et al. 2021) is the fifth generation of the ECMWF reanalysis products. Monthly and hourly variables such as surface winds and winds and geopotential height at 925, 850, and 600 hPa on a resolution of $0.25° \times 0.25°$ are used to understand circulation features associated with dust emissions and long-range transport.

Hourly and monthly volumetric soil water of the top layer (i.e., 0–7cm) with a spatial resolution of $0.1° \times 0.1°$ is used to examine land surface conditions associated with dust emissions. Daily values are averaged from hourly data. ERA5 is the first ECMWF reanalysis to incorporate soil moisture retrievals from C-band scatterometer instruments onboard European Remote Sensing satellites-1,2 (ERS-1, 2) and Meteorological Operational satellites A, B (MetOp-A, B) (Piles et al. 2019; Hersbach et al. 2020; Agutu et al. 2021; Muñoz-Sabater et al. 2021). Although its soil moisture product does not incorporate ground-based observations and lacks sufficient spin-up time to accurately represent deep soil moisture, ERA5 soil moisture estimates show high skill for shallow soil moisture in regions where gauge measurements are lacking, such as western Africa (Brocca et al. 2020; Beck et al. 2021; Muñoz-Sabater et al. 2021).

3.2 Jet Indices

Both the African easterly jet (AEJ) and the Caribbean low-level jet (CLLJ) are found to affect the westward propagation of African dust plumes (Prospero and Carlson 1981; Pu and Jin 2021). The extremely enhanced easterly jets also contributed to the development of the "Godzilla" dust event in June 2020 (Pu and Jin 2021). Here we examine how these jets may affect the formation of the extreme African dust plume in 2015. We use jet indices to quantify the magnitude of the jets, which are calculated by averaging easterly wind speed over their climatological locations, similar to regions selected in prior papers (Cook 1999; Wang 2007; Leroux and Hall 2009; Martin and Schumacher 2011). Following Pu and Jin (2021), the CLLJ index is calculated by averaging ERA5 925 hPa easterly wind between 11°N – 17°N and 70°W – 80°W from ERA5, and the AEJ index is calculated by averaging ERA5 600 hPa easterly wind speed between 10°N – 15°N and 30°E – 10°W.

3.3 Identify Extreme Trans-Atlantic Dust Events

We first use aerosol extreme events (AEE; Pu and Jin 2021) to identify high dust loading days over the tropical North Atlantic and over western North Africa. An AEE is defined when the regional mean daily MODIS AOD is above the 90th percentile of daily AOD centered on a 15-day window during 2003–2022 in boreal summer (June–August). The duration of an AEE is defined as the number of consecutive days (≥1) that meet the criteria, while the magnitude of an AEE is calculated by averaging AOD during the event. Following Pu and Jin (2021), we calculated AEEs over the tropical North Atlantic (8°N – 25°N, 18°W – 90°W; see location in Figure 1a) and over the western North Africa dust source region (8°N – 25°N, 18°W – 5°W; see Figure 1a) for JJA 2003–2022. During boreal summer peak dust activities are mainly located in western North Africa, extending from

the Mauritanian coast to the Mali–Mauritania border and Mali–Algeria border (Goudie and Middleton 2001; Prospero et al. 2002; Engelstaedter et al. 2006; Engelstaedter and Washington 2007). The averaging regions largely capture the westward

280   transport pathway of African dust in summer, and the results are very similar to that of 2003–2020 (Pu and Jin 2021; their Fig. 2). Over the tropical North Atlantic region, the AEE in June 2020 has the highest magnitude of AOD in the record with a duration of 12 days (not shown), and the June 2015 event is the second highest, with a duration of six days (Figure 1c). Over the dust source region in western North Africa, a one-day AEE event on June 13 is found, with a moderately high AOD of 0.74 (Fig. 1b), weaker than that in June 2020 (a six-day AEE of 0.90) and slightly below the mean of AEEs over western North

285   Africa (Fig. 1d). Note that only days where the averaging area has less than 30% missing AOD values are used in AEE calculations, and this criterion mainly affects the AEEs over land (Fig. 1b). Slightly increasing or reducing the missing value threshold (e.g., to 20% or 40%) does not change the AEE days over the ocean.
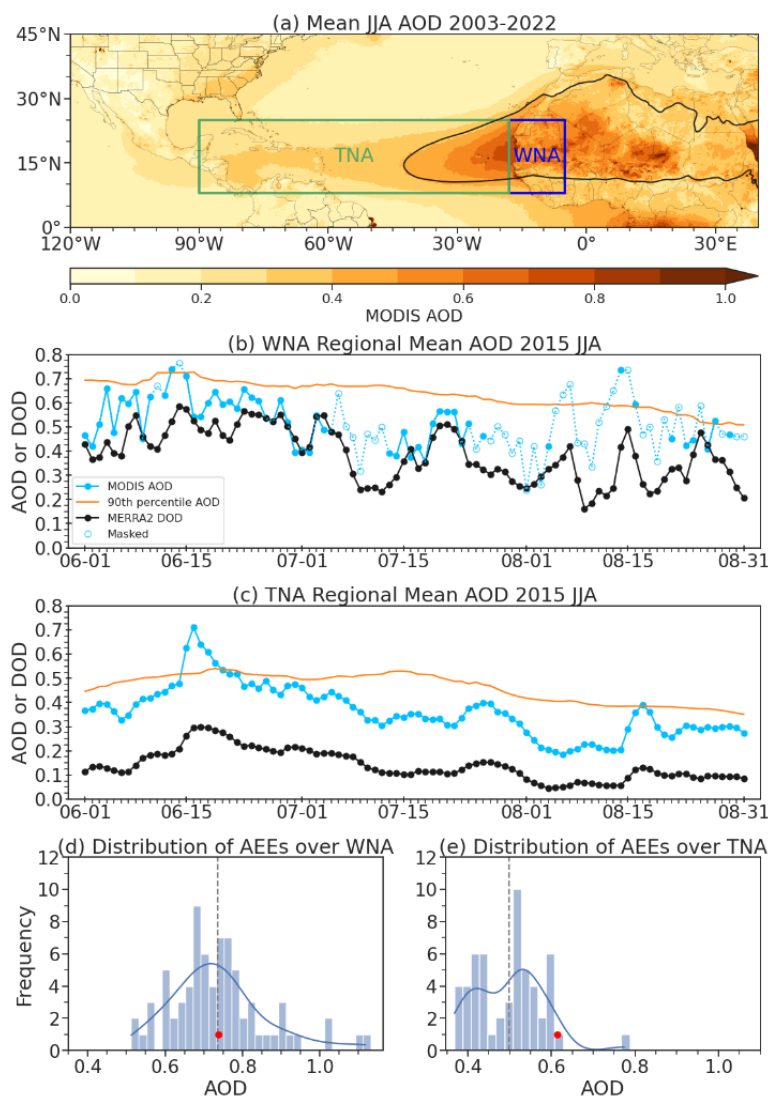
Figure 1. (a) Climatology of MODIS AOD in JJA from 2003 to 2022. Regions with MERRA-2 DOD ≥ 0.3 are contoured in black.
290 **The averaging area over the tropical North Atlantic (TNA; 8°N - 25°N, 18°W - 90°W) and western North Africa (WNA; 8°N - 25°N,**
18°W - 5°W) regions are marked by green and blue boxes, respectively. Regional mean daily MODIS AOD (blue) and MERRA-2
DOD (black) in JJA 2015 over (b) western North Africa and (c) the tropical North Atlantic. The 90th percentile of daily MODIS
AOD in JJA (2003–2022) is shown in orange. Filled (empty) circles represent days with less than (more than) 30% missing values
within the regional boxes. Distribution of AEEs from 2003-2022 over (d) WNA, and (e) TNA. Red dots mark values of the June 2015
295 **event, and the vertical dashed lines denote means of AEEs over WNA and TNA.**

While AEEs capture the maxima AOD during the event (Figures 1b-c), a trans-Atlantic event usually lasts more than a week
as it takes about seven days for African dust to reach the Caribbean and 10–12 days to reach the continental U.S. (Ott et al.
1991; Haarig et al. 2017; Chen et al. 2018). Thus, we also use an AOD Hovmöller diagram over the tropical North Atlantic
300 that shows the westward propagation of dust plume (Figure 2) and a daily AOD plot (Figure 3) to identify the beginning and
ending dates of the event. We found that the extreme dust event started around 12 June and ended around 23 June 2015.
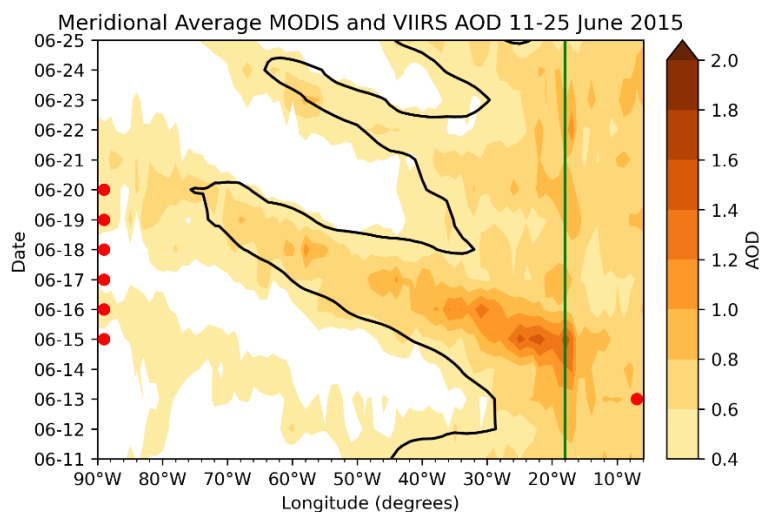
Figure 2. Hovmöller plot of the meridional averaged MODIS and VIIRS AOD from 8°N - 25°N across the tropical North Atlantic
from 11 June to 15 June 2015. Only AOD above 0.4 is shown. The black contour denotes the areas where MERRA-2 DOD ≥ 0.3.
305 **The green line denotes 18°W, the dividing line between the averaging boxes shown in Figure 1. Red dots mark the dates of AEEs**
over the tropical North Atlantic (left) and over western North Africa (right).

4 Results

4.1 Features of the extreme trans-Atlantic dust event in June 2015

Figure 3 shows the daily mean AOD averaged between MODIS and VIIRS from 11 to 25 June 2015. The extreme dust event
310 began around 12 June, and on 12-13 June AOD reached the 95th percentile over the western Guinea coast. On the 14th AOD

exceeded 2.0 over the borders of Mauritania, Mali, and Senegal (Figs. 3b-d). The plume was then rapidly advected out of the source region and into the tropical North Atlantic on 15 June. AOD over the west coast and tropical North Atlantic reached 4.95 (Fig. 3e). During its westward transport, large portions of the plume show AOD above the 95th percentile value in JJA over 2003–2022 and above the 99th percentile in some regions over the tropical North Atlantic (Figure S1). The dust plume

315   arrived at the Caribbean Sea around 17 June (Fig. 3g) and passed through the region and began to split around 21 June (Fig. 3k). The northern branch of the plume was advected northward and dispersed across the Gulf region and the southern central and eastern U.S., while the southern branch of the plume travelled across the Guatemala Basin to the eastern tropical Pacific Ocean (Figs. 3l-o). The plume was still quite strong even after it passed into the Pacific, with daily AOD above the 99th percentile (Figs. S1m-o). Previous studies found that the westward movement of African dust in summer can reach 100 °W

320   (e.g., Vuolo et al. 2009; Adams et al. 2012). In this extreme event, the African dust plume travelled as far as 120 °W and beyond (Figs. 3l-o).
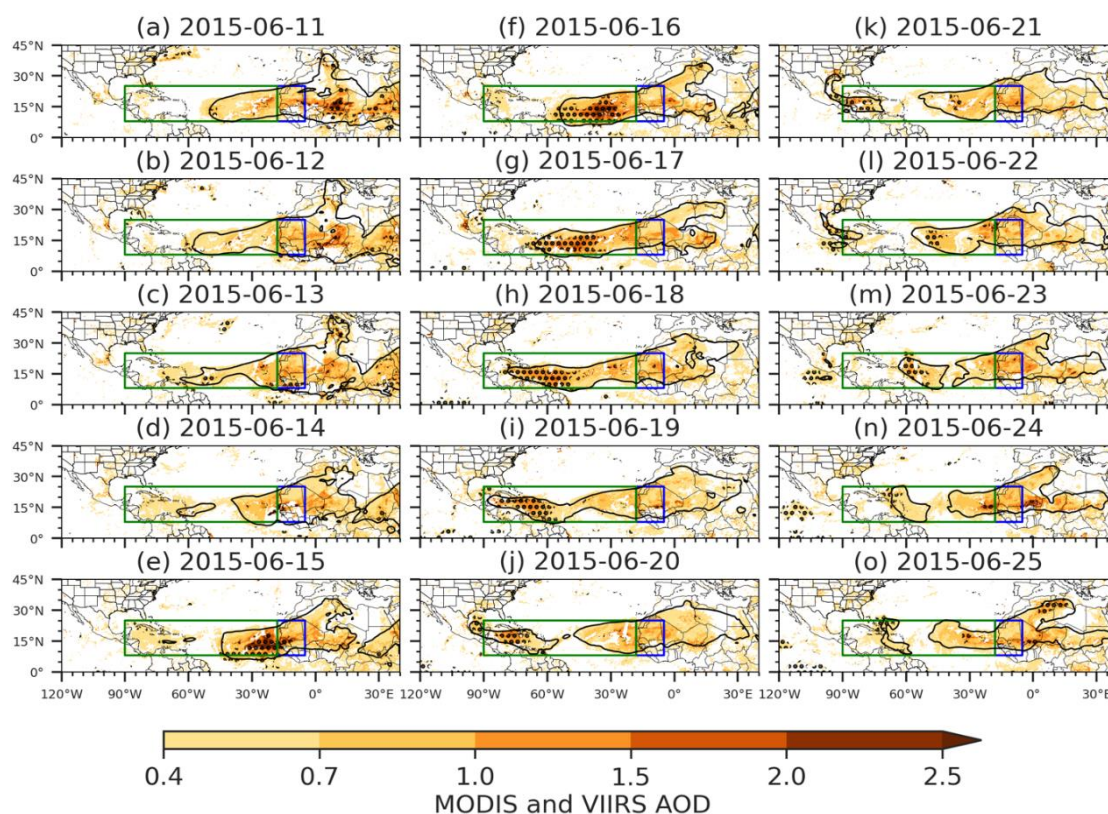
Figure 3. Combined MODIS and VIIRS AOD from 11 to 25 June 2015. Only AOD above 0.4 is shown. Black contours denote the boundary where MERRA-2 DOD ≥ 0.3. Dots represent regions where MODIS AOD is ≥ 95th percentile (with reference to daily

325   **MODIS AOD in JJA from 2003 to 2022 at each grid point). The green and blue boxes correspond to the averaging areas over the tropical North Atlantic and western North Africa, respectively.**
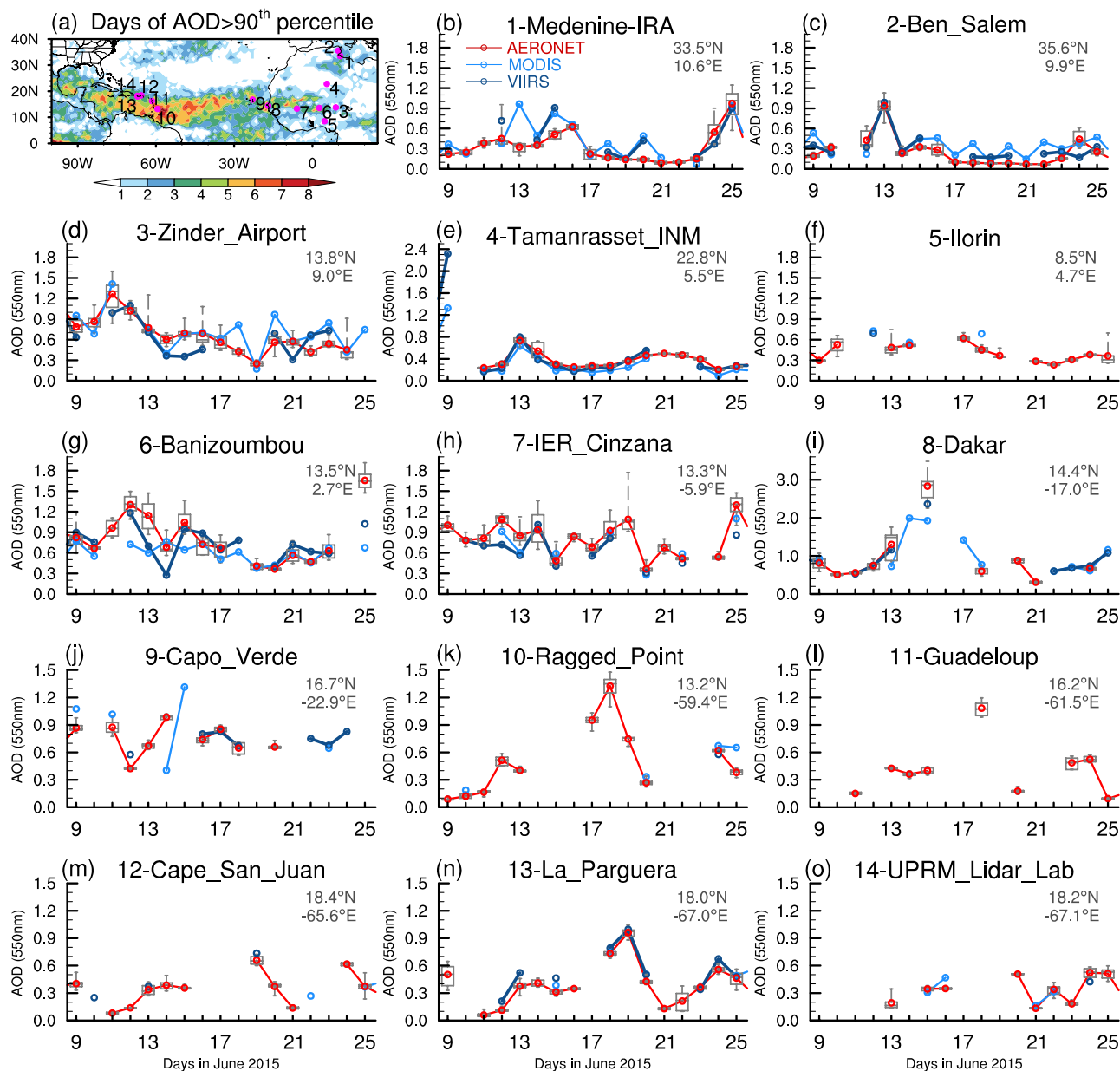
Figure 4. (a) Number of days when daily MODIS AOD greater than the 90th percentile of JJA daily values (2003–2022) during 12–24 June 2015. Locations of 14 AERONET stations are shown in magenta. (b)–(o) Daily AOD from AERONET (red), MODIS (light blue), and VIIRS (deep blue) during 9–25 June 2015. Sub-daily values of AERONET AOD are shown in the box in grey, with the upper, lower, and middle bars showing the 25th and 75th percentiles and median of the data and whiskers extending from the minimum to the maximum. The red circles denote the daily mean of AERONET AOD. The latitudes and longitudes of AERONET sites are shown on the top right.

330

335   The evolution of AERONET AOD records (Figure 4) largely resembles satellite AOD (Fig. 3). For sites over North Africa, AOD values slightly enhanced before or around 13 June 2015, with magnitudes largely less than 1.6, which is consistent with the findings in Fig. 1 that dust emissions over land were enhanced but not extremely high. Over the coastal region, the daily maximum AOD at Dakar reached 3.5 on 15 June (Fig. 4i) as the dust plume propagated toward the ocean (Fig. 2e). MODIS and VIIRS AOD showed a similar peak around 15 June at Dakar and Capo Verde sites, but in a weaker magnitude (Figs. 4i-
340   j). When the dust plume reached the Caribbean Basin, AERONET AOD increased to 1.5 at the Ragged Point site on 18 June and 1.0 at the La Parguera site on 19 June. In comparison to AERONET records during the "Godzilla" event (Yu et al. 2021), daily mean AOD values were about 0.7 lower over the African coastal region and eastern tropical Atlantic (Dakar vs. Capo Verde) and about 0.3~0.8 lower over the Caribbean Basin at Ragged Point, Guadeloupe, and La Parguera sites.

345   CALIOP total attenuated backscatter shows the vertical profiles of dust plume (Figure 5). The plume was more compact and had a greater vertical extent (from 1.5 to 6 km) at its origin over western North Africa during June 13–14, 2015 (e.g., in between sampling points B and C in Fig. 5a-b). The high plume top over the source region is consistent with a previous study by Petit et al. (2005) who suggested that a minimum dust layer altitude of 3 km off the west coast of North Africa is necessary for African dust plumes to completely cross the Atlantic and enter the Caribbean, as dust plumes descend during westward
350   transport. This descent is a balance between the convection in the underlying marine layer and the subsidence of anticyclonic air of the NASH (Petit et al. 2005). As the plume travelled westward over the tropical North Atlantic, it slowly subsided and weakened, consistent with previous studies (Braun 2010; Adams et al. 2012; Groß et al. 2015; Weinzierl et al. 2017), although the rate of descent was somewhat slower than 500 m day^{-1} during the June 2020 event (Yu et al. 2021). By 18 June the plume over the western tropical North Atlantic was primarily between 2 and 5 km (Fig. 5f). Because CALIOP data were missing
355   between 19 June and 28 June 2015, it is not entirely clear whether the descending rate increased as the plume propagated across the Caribbean Basin.
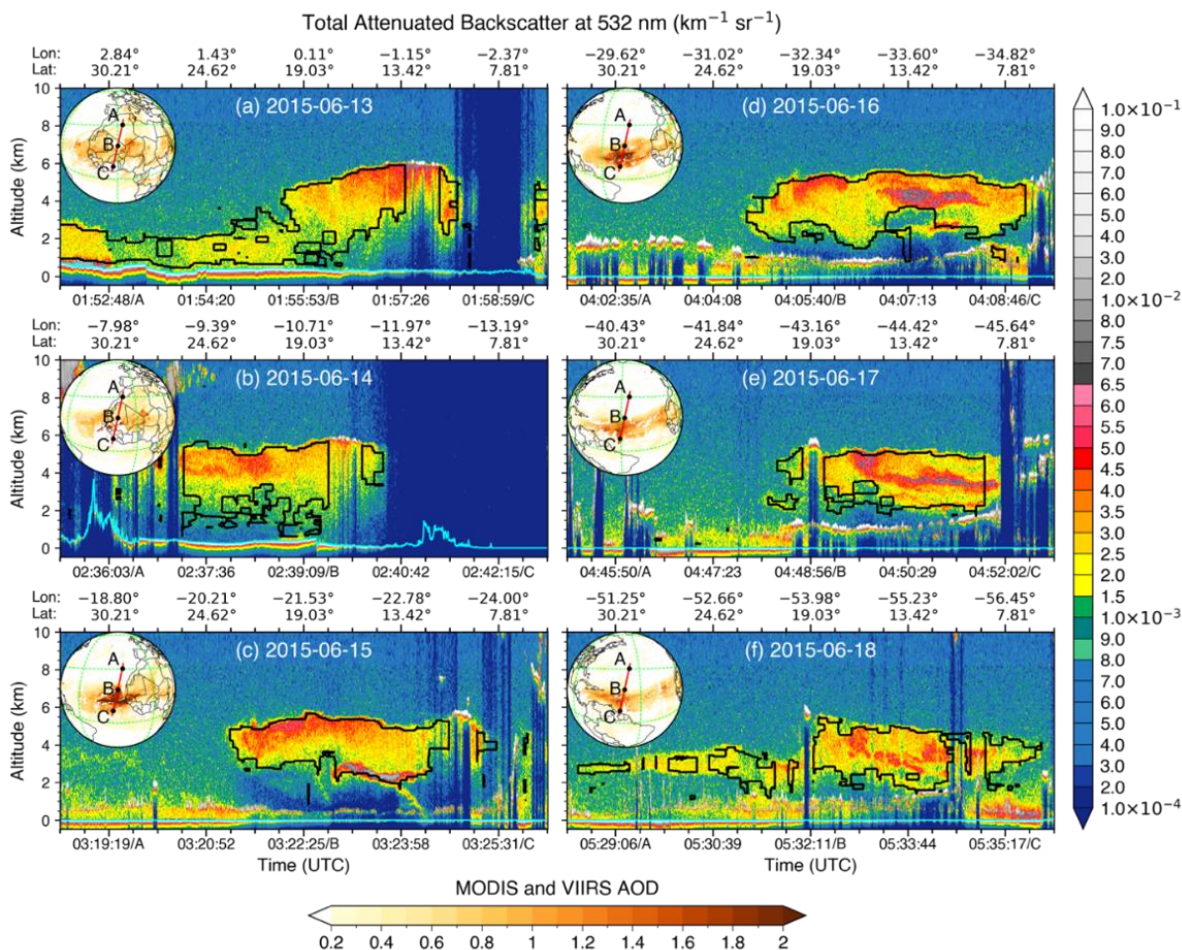
Figure 5. CALIOP 532 nm total attenuated backscatter (km^{-1} sr^{-1}) for 13–18 June 2015. The satellite tracks (red lines) are displayed in the inset at the upper left of each panel with sampling points (A–C) corresponding to the x-axis of the cross-section and brown shading showing MODIS-VIIRS averaged AOD. Black contours denote dust aerosols (depolarization ratio ≥ 0.2). Surface elevation is indicated by cyan lines.

4.2 Circulation conditions associated with the 2015 extreme dust event
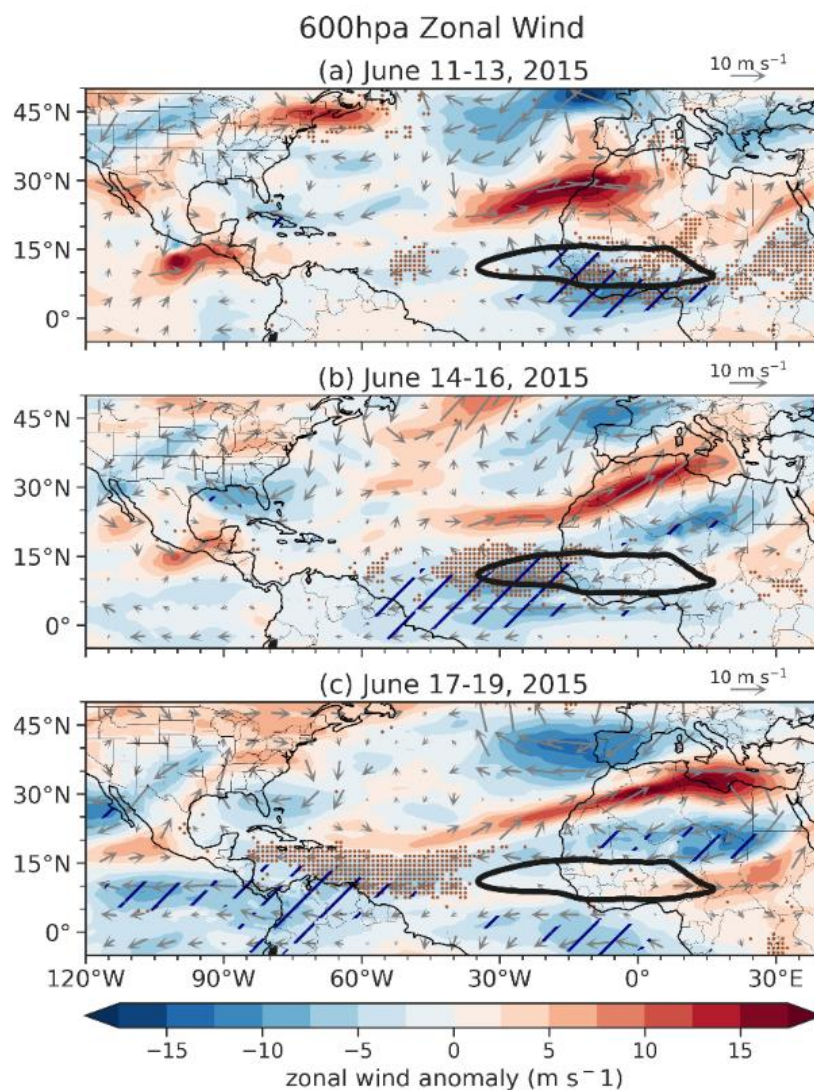
Figure 6. Anomalies of three-day mean 600 hPa winds (vectors; m s⁻¹) and zonal wind speed (shading; m s⁻¹) from 11 to 19 June 2015 with reference to the 1979–2022 climatology in June. Black contours show the climatological location of the African easterly jet (AEJ; denoted by zonal wind speed of -11 m s⁻¹). Hatches represent regions where easterly wind speeds ≥ 95th percentile (with reference to the absolute magnitude of three-day mean zonal wind speed in June from 1979 to 2022 at each grid point). Dots represent regions where MODIS AOD ≥ 95th percentile (with reference to daily AOD in JJA from 2003 to 2022 at each grid point) and ≥ 0.6.

In this section, we will examine the large-scale circulation patterns associated with the westward transport of the extreme African dust plume. Over western North Africa and the eastern North Atlantic, the AEJ centered around 600 hPa plays an important role in transporting African dust westward (Prospero and Carlson 1981; Jones et al. 2003; Schepanski et al. 2017;

Pu and Jin 2021; Yu et al. 2021), with a stronger jet associated with higher AOD over the tropical North Atlantic (Pu and Jin 2021). Figure 6 shows anomalies of three-day averages of zonal wind speed at 600 hPa around the onset of the event (11–13

375 June) to the time when the dust plume reached the Caribbean Basin (17–19 June). The black contour shows the climatological location of the jet, and the hatched area denotes regions where zonal wind speed is above the 95th percentile in June during 1979–2022 in the ERA5 reanalysis. During 11–13 June, the easterly wind anomalies were located between 0°N and 17°N over the jet core region and the Guinea coast. The jet continued to intensify during 14–19 June, advecting the dust plume westward to the central tropical North Atlantic (Figs. 6b-c). The magnitude of the AEJ right before and at the beginning of the event

380 (11–16 June) was 16.8 m s^{-1}, which is the 4th strongest for this week from 1979 to 2022 (Fig. S2a), greatly favoring the export and westward transport of African dust.

When the dust plume propagated to the central to western tropical North Atlantic, the anticyclonic flow of the NASH can further transport it westward. Figure 7a-c shows three-day averages of the geopotential height and wind anomalies at 850 hPa.

385 The NASH had a westward extension from its climatological location toward the Gulf of Mexico and the southeastern U.S. from 17 to 25 June 2015. The related easterly and southerly wind anomalies further steered the dust plume toward the continental U.S. The westward extension of the NASH along with the reduced height over the tropical eastern Pacific further increased the meridional pressure gradient over the Caribbean Basin and strengthened the CLLJ at 925 hPa (Figs. 7d-f). In fact, the magnitude of the CLLJ during 17–22 June (~18.3 m s^{-1}) is the strongest for the same period from 1979 to 2022 in the

390 ERA5 reanalysis (Fig. S2b). Such a high magnitude of the jet is consistent with the extremely enhanced geopotential heights to the north of the Caribbean Basin and reduced heights to the south (hatched regions in Figs. 7a-c). The greatly strengthened CLLJ facilitated the westward transport of the African dust across the Caribbean Basin. The extreme easterly jet further advected part of the plume into the eastern Pacific, while the remainder of the plume was carried northward to the U.S. by the anticyclonic flow (Figs. 7e-f).

Figure 7. (a)-(c) Anomalies of three-day mean 850 hPa geopotential height (shading; gpm) and winds (vectors; m s^{-1}) with reference to the 1979-2022 climatology in June. Black contours show the climatological location of the North Atlantic subtropical high (NASH; (denoted by the 1560 gpm contour following Li et al. 2011), and green contours mark the three-day mean location of the NASH. Hatchings represent the top ($\geq 95^{th}$; backward) and bottom ($\leq 5^{th}$; forward) percentiles of geopotential height (with reference to June three-day mean values from 1979-2022 at each grid point). (d)-(f) Anomalies of three-day mean 925 hPa winds (vector; m s^{-1}) and zonal wind speed (shading; m s^{-1}) with reference to the 1979-2022 climatology in June. Black contours show the climatological location of the Caribbean low-level jet (CLLJ; denoted by the zonal wind speed contour of -11 m s^{-1}), and green contours mark the three-day mean location of the CLLJ. Hatchings represent regions where easterly wind speed $\geq 95^{th}$ percentile (with reference to the absolute magnitude of three-day zonal wind in June from 1979-2022 at each grid point). In all panels, dots represent MODIS AOD $\geq 95^{th}$ percentile (with reference to three-day mean AOD in JJA from 2003 to 2022 at each grid point) and ≥ 0.6.

Overall, the circulation patterns in the June 2015 event are largely consistent with the findings of Pu and Jin (2021), who showed that the enhanced AEJ and CLLJ and the westward extension of the NASH all contribute to the long-range transport of African dust to the tropical North Atlantic and the Caribbean Basin. The extremely high magnitudes of the AEJ and CLLJ in this event also suggest that circulation extremes played important roles in the formation of high dust loading over the ocean.

One unique feature of the June 2015 event is the extremely strong CLLJ that transported a portion of the dust plume to the eastern Pacific, so fewer dust particles were being advected to the U.S.

4.3 Anomalous dust emissions
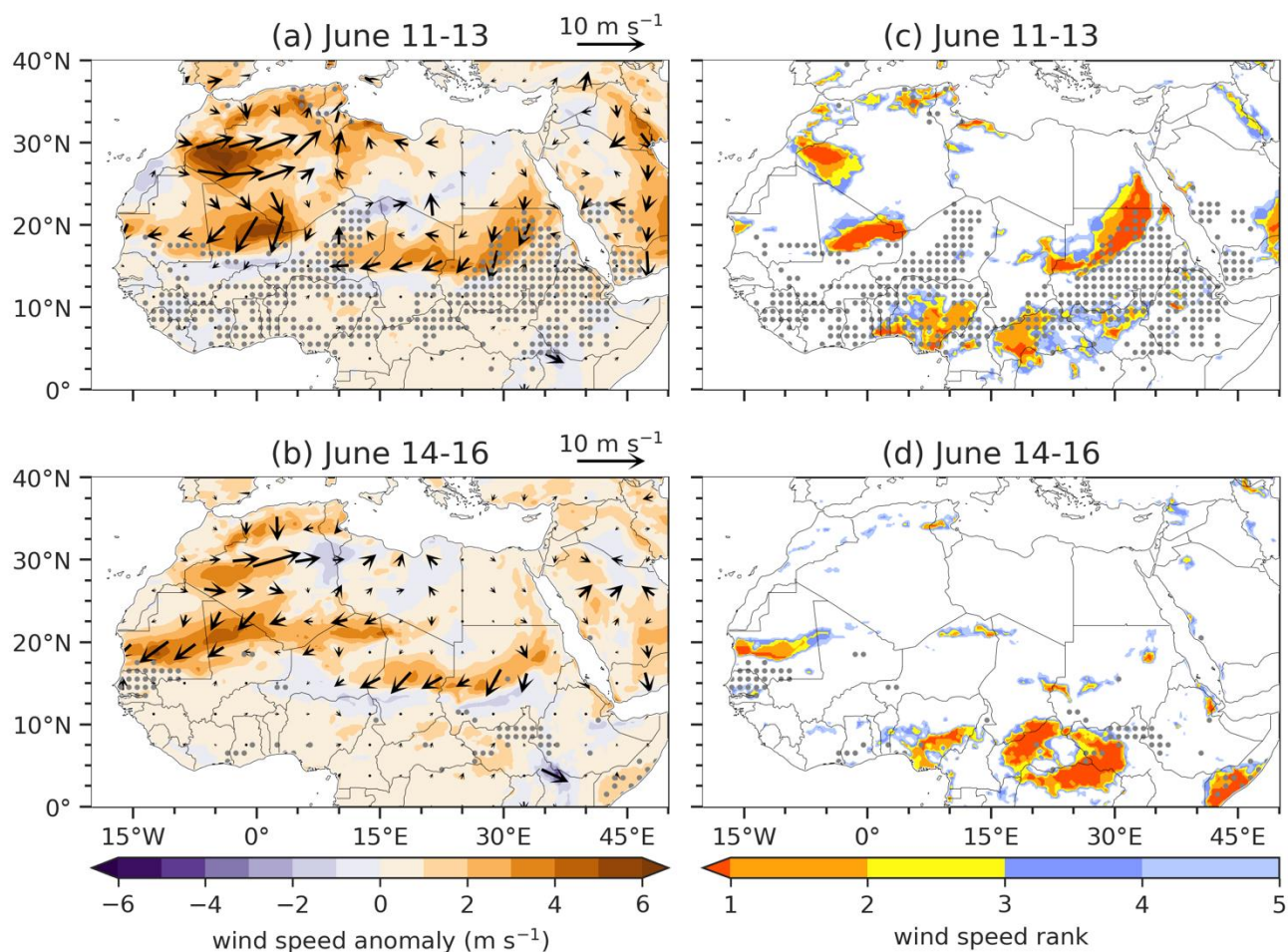
Figure 8. (a)-(b) Anomalies of 10 m winds (vectors; m s⁻¹) and wind speeds (shading; m s⁻¹) averaged over 11–13 June, and 14–16 June 2015 (with reference to the 1979-2022 climatology in June). (c)-(d) Ranking of daily surface wind speed averaged over 11–13 June and 14–16 June 2015, with reference to the corresponding three-day averages over 1979–2022 (44 years). Only wind speed rank 1– 5 (i.e., top five strongest) are shown. Areas with MODIS AOD ≥ 95th percentile (with reference to three-day mean AOD in JJA from 2003 to 2022 at each grid point) and ≥ 0.6 are dotted in grey.

As shown in Fig. 1b, the extreme trans-Atlantic dust event is associated with a one-day AEE on 13 June over western North Africa, which indicated enhanced dust emissions over source regions at the beginning of the event. To understand the factors that increased dust emissions we first examine local surface wind speed, which has long been related to dust emissions in North Africa (e.g., Gillette et al. 1980; Helgren and Prospero 1987; Engelstaedter and Washington 2007; Cowie et al. 2015; Evan et al. 2016). Figure 8 shows three-day averages of 10m surface wind anomalies during 11–16 June 2015 and the rank of the top five strongest surface wind speeds during the same days from 1979–2022 over North Africa. Surface wind speeds are greatly intensified over eastern Mali to Mali-Algeria border, western Algeria, and southern Egypt to north Sudan (Figs. 8a-b). The magnitude of the surface wind speed ranked the highest or among the top five over summertime active dust source regions in central to eastern Mali (Fig. 8c) and Mauritania (Fig. 8d). High percentile AOD (grey dots) are largely located downstream of regions of extreme surface winds.
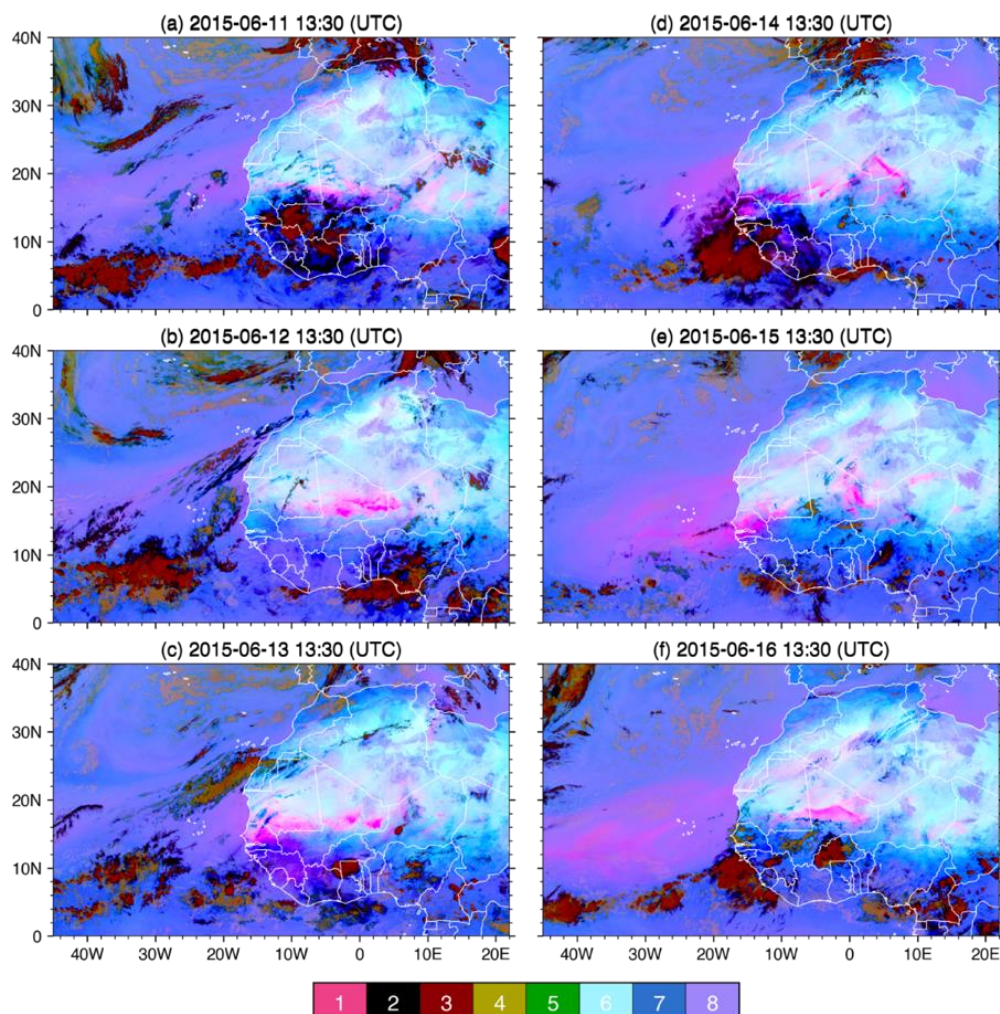
Figure 9. (a)-(f) Dust RGB from SEVIRI at 13:30 UTC from 11 to 16 June 2015. Dust plumes are denoted by magenta shading (color 1), while deep convection is shown in dark red (color 3). Cirrus clouds, mid-level clouds, thin cirrus, hot sandy desert, low-level humid air, and low-level dry air are shown in black, dark golden, green, light cyan, blue, and purple, respectively.

435

The anomalously strong surface wind-induced dust emissions are also captured by the SEVIRI dust RGB images (Figure 9). While the dust emissions in Mali (magenta) on 11 June 2015 were likely affected by the outflow of downdrafts generated by the mesoscale convective systems (MCSs) over southern to central Mali and Burkina Faso (dark red; Fig. 9a), the enhanced dust emissions over central Mali, Mali-Algeria-Niger border, and Mauritania during 12-16 June (Figs. 9 b-f) are largely

440 collocated with the strong surface anomalies (Fig. 8c, d). On 14 June, a coastal MCS also contributed to the enhancement of dust emissions in Mauritania (Fig. 9d).

In addition to increased surface wind speeds, land surface conditions such as dry soil due to precipitation deficit and reduced vegetation coverage also favor dust emissions (Gillette et al. 1980; Engelstaedter et al. 2006; Cowie et al. 2014; Kim et al.

445 2017; Pu and Ginoux 2018b). Figure 10 shows three-day averages of soil moisture anomalies from ERA-5 and NDVI anomalies from MODIS across North Africa. Soil moisture decreased over large areas in the Sahara and Sahel. In the southern Sahel soil moisture anomaly reached -0.1 m^3 m^{-3} (about -40%), below the 5th percentile during June 2003-2022 (Fig. 10a-b), likely as a result of decreased rainfall (Fig. S3). Note that the precipitation reduction over the tropical North Atlantic (Fig. S3) also helped maintain the high dust loading over the ocean by minimizing the scavenging of fine dust aerosols over the southern

450 part of the dust plume around 5–10°N. Vegetation decayed almost over the same areas where soil moisture was greatly reduced, reaching the lower 5th percentile (Fig. 10c-d), even the lowest 1st percentile in some areas (not shown), favoring wind erosion in the region.
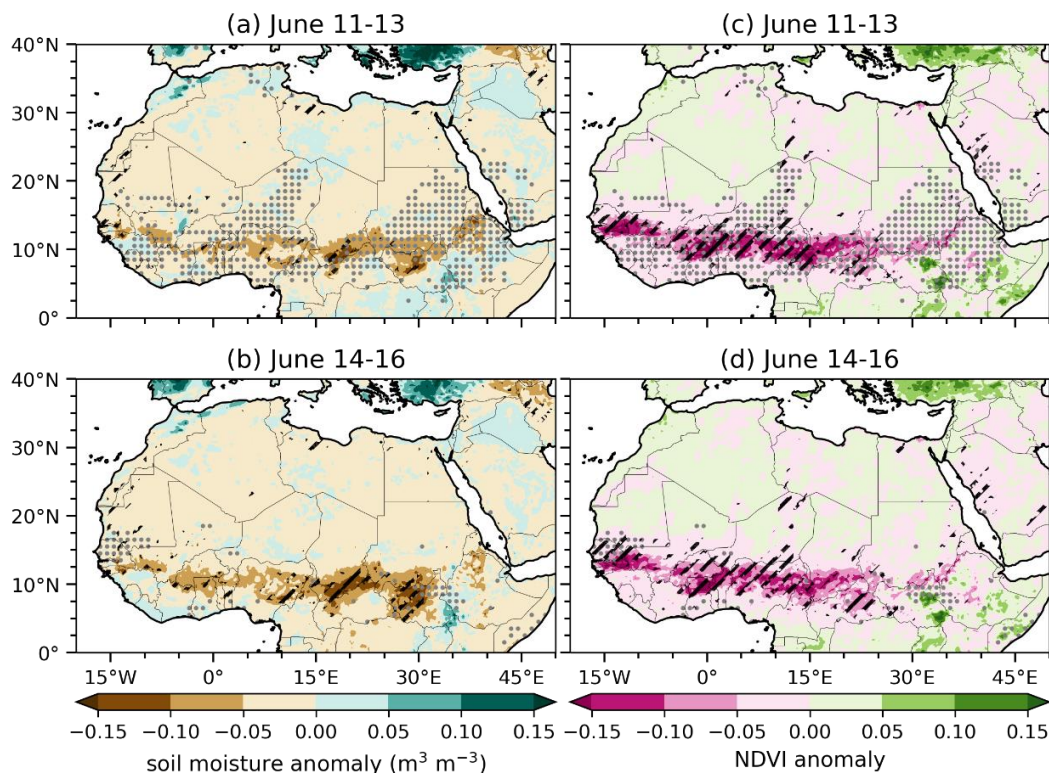
Figure 10. (a)-(b) Anomalies of ERA5 first-layer (top 7 cm) volumetric soil water (m^3 m^{-3}; with reference to the 1979-2022 climatology

455 **in June) averaged over 11–13 June and 14–16 June 2015. Hatchings represent soil water ≤ 5th percentile (with respect to June three-day means from 2003-2022 at each grid point). (c)-(d) Anomalies of MODIS NDVI (with reference to the 2003-2022 climatology in**

June) averaged over 11–13 June and 14–16 June 14–16 2015. Hatchings represent NDVI ≤ 5th percentile (with respect to JJA three-day means from 2003-2022 at each grid point). Dots represent regions where MODIS AOD is ≥ 95th percentile (with reference to three-day mean MODIS AOD in JJA from 2003 to 2022 at each grid point) and ≥ 0.6.

460 **4.4 Impacts of the 2015 trans-Atlantic extreme dust event**

4.4.1 Radiation Impacts

The perturbation of the June 2015 extreme African dust plume on radiative fluxes at the TOA and surface are examined using CERES clear-sky daily data. Figure 11a shows anomalies of regional mean shortwave (SW) and longwave (LW) fluxes over the eastern tropical North Atlantic (8°N–25°N, 18°W–42°W), along with MODIS AOD in June 2015. At the surface, when
465 regional mean AOD reached the maximum of ~1.1 on 16 June, the reduction of SW flux also reached a peak, at about –25.3 W m^{-2}, while LW flux had a weak warming anomaly of about 3.5 W m^{-2} associated with scattered and emitted LW radiation by the warm SAL. Consistent with previous studies (e.g., Tegen et al. 1996), changes in radiative fluxes at the TOA were much smaller than that at the surface, with about 3.0 W m^{-2} LW warming and –1.0 W m^{-2} SW cooling, although no clear maxima were found when AOD peaked. Both the sign and magnitude are consistent with previous studies of the TOA radiative effects
470 of African dust over the Atlantic (e.g., Yu et al. 2006; Yorks et al. 2009). The SW cooling at the TOA is associated with the increased reflected solar flux due to the bright dust layer above the dark ocean surface, while the LW warming is often related to the absorption of outgoing LW by the dust layer but may be also affected by the moisture content in the atmosphere.
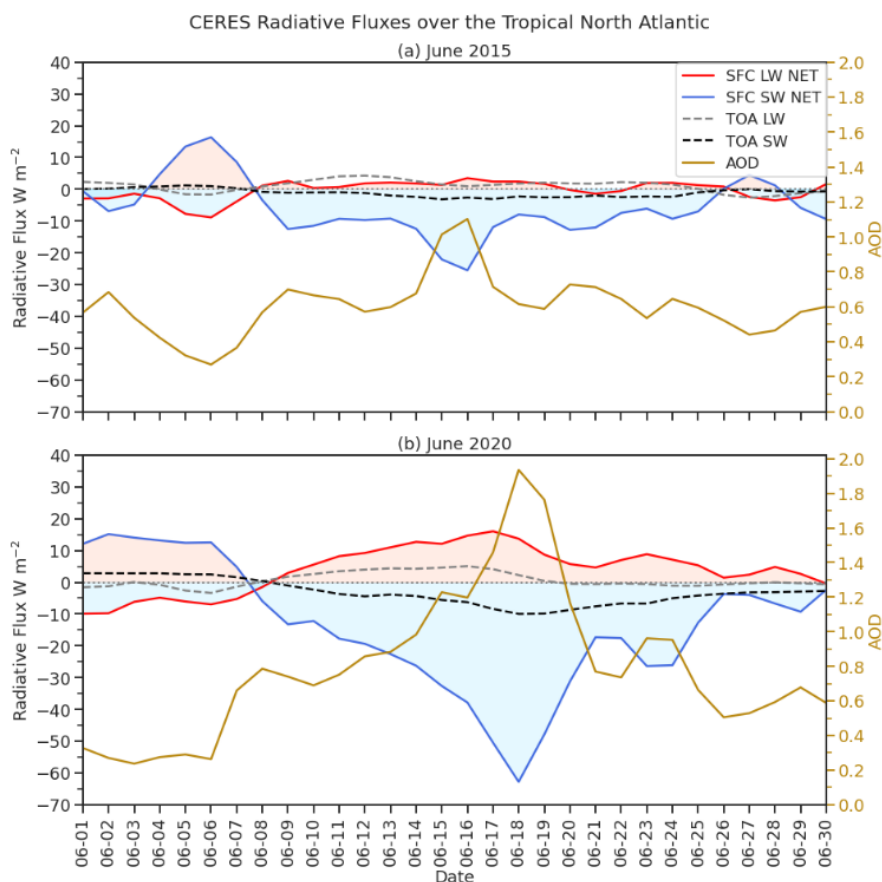
Figure 11. Time series of CERES clear-sky radiative fluxes (W m^{-2}) and MODIS AOD in (a) June 2015 and (b) June 2020 averaged over the eastern tropical North Atlantic between 8°N – 25°N and 18°W – 42°W. Anomalies (with reference to the 2003-2022 climatology in June) of net shortwave (SW) and longwave (LW) fluxes at the surface are shown in solid blue and red lines, respectively. Reflected SW and outgoing LW fluxes at the top of the atmosphere (TOA) are shown in dashed black and grey, respectively. Positive (negative) values indicate downward (upward) fluxes. Red (blue) shading denotes the warming (cooling) effect at the surface. AOD is shown in gold on the right y-axis.

Fig. 11b shows the radiative fluxes of the June 2020 event for comparison. With a more intense dust plume and a higher AOD of up to 1.9 on 18 June 2020, surface SW flux reached – 62.0 W m^{-2}, more than two times the perturbation in the June 2015 event. The corresponding surface LW flux perturbation is also about two times stronger. Also different from the June 2015 event is that the TOA SW flux showed a minimum (~ –10.0 W m^{-2}) when AOD reached a maximum, while the TOA LW warming effect peaked a bit early before the maximum of AOD. The net surface LW and SW flux values shown here are comparable to the changes in surface radiative fluxes over the eastern Atlantic found by Francis et al. (2022; their Fig. 4).
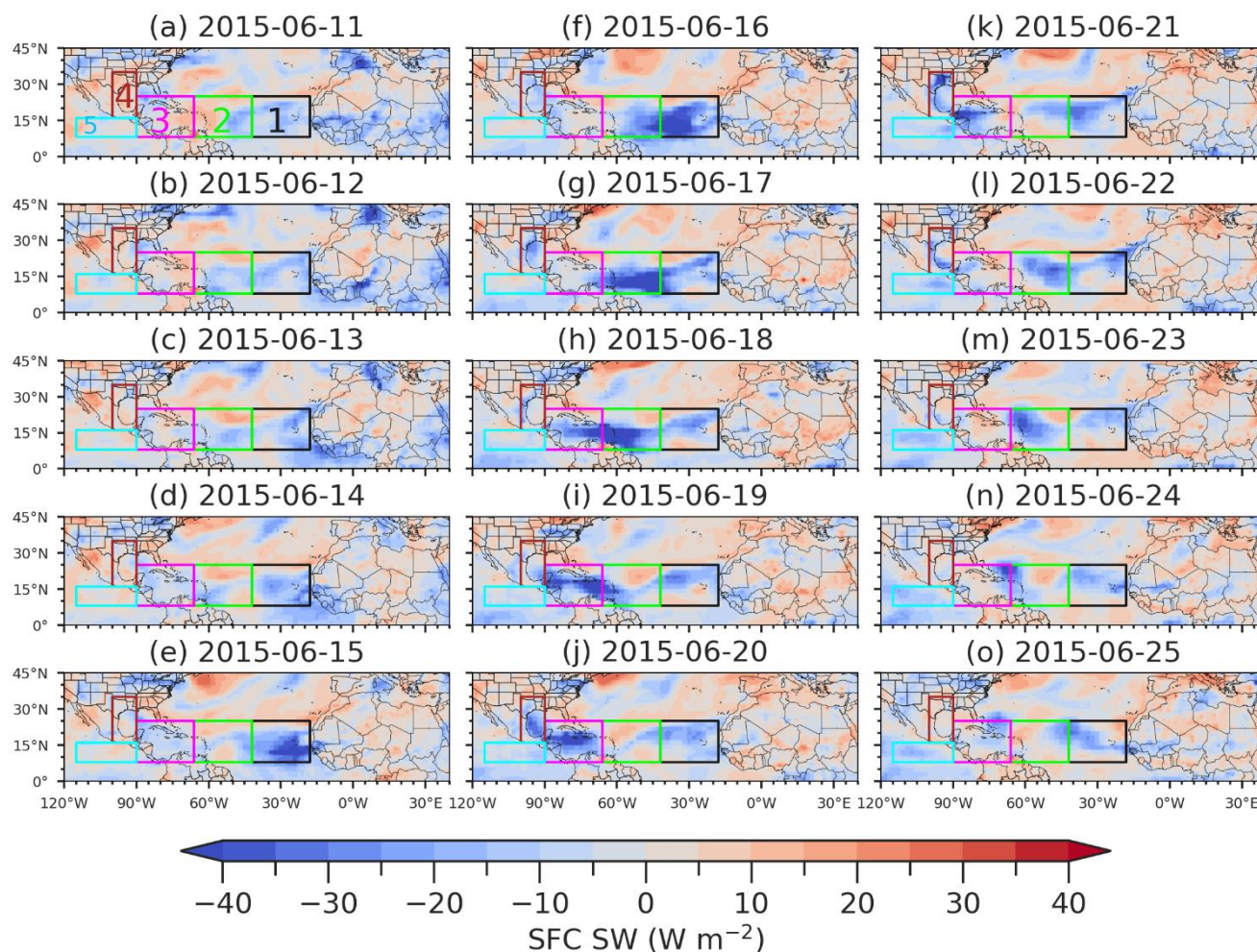
Figure 12. Anomalies (with reference to the June climatology over 2003-2022) of CERES clear-sky net shortwave fluxes at the surface (W m⁻²). Boxes represent averaging regions to track the changes in radiative flux due to the propagation of the African dust plume.
490 **Region 1 (black) is between 8°N – 25°N and 18°W –42°W, Region 2 (green) is between 8°N – 25°N and 42°W – 66°W, Region 3 (magenta) is between 8°N –25°N and 66°W – 90°W, Region 4 (brown) is between 16°N – 35°N and 90°W – 100°W, and Region 5 (cyan) is between 8°N – 16°N and 90°W – 115°W.**

The spatial pattern of anomalous net surface SW flux during the June 2015 event is shown in Figure 12. The propagation of
495 the negative anomalies of surface SW fluxes is quite consistent with the westward movement of the dust plume (Fig. 3), as expected; and the large reductions are over the regions where AOD reached the 95th percentile (dotted areas in Fig. 3), with a magnitude of up to –73.6 W m^{-2} in the eastern tropical Atlantic on 16 June and reached -56.6 W m^{-2} over the Caribbean Basin

on 21 June. Note that during 21–25 June, the reduction of surface net SW extended to the eastern tropical Pacific as the dust plume was advected to the region by the extremely strong CLLJ, with a magnitude of up to –28.4 W m^{-2}.

500
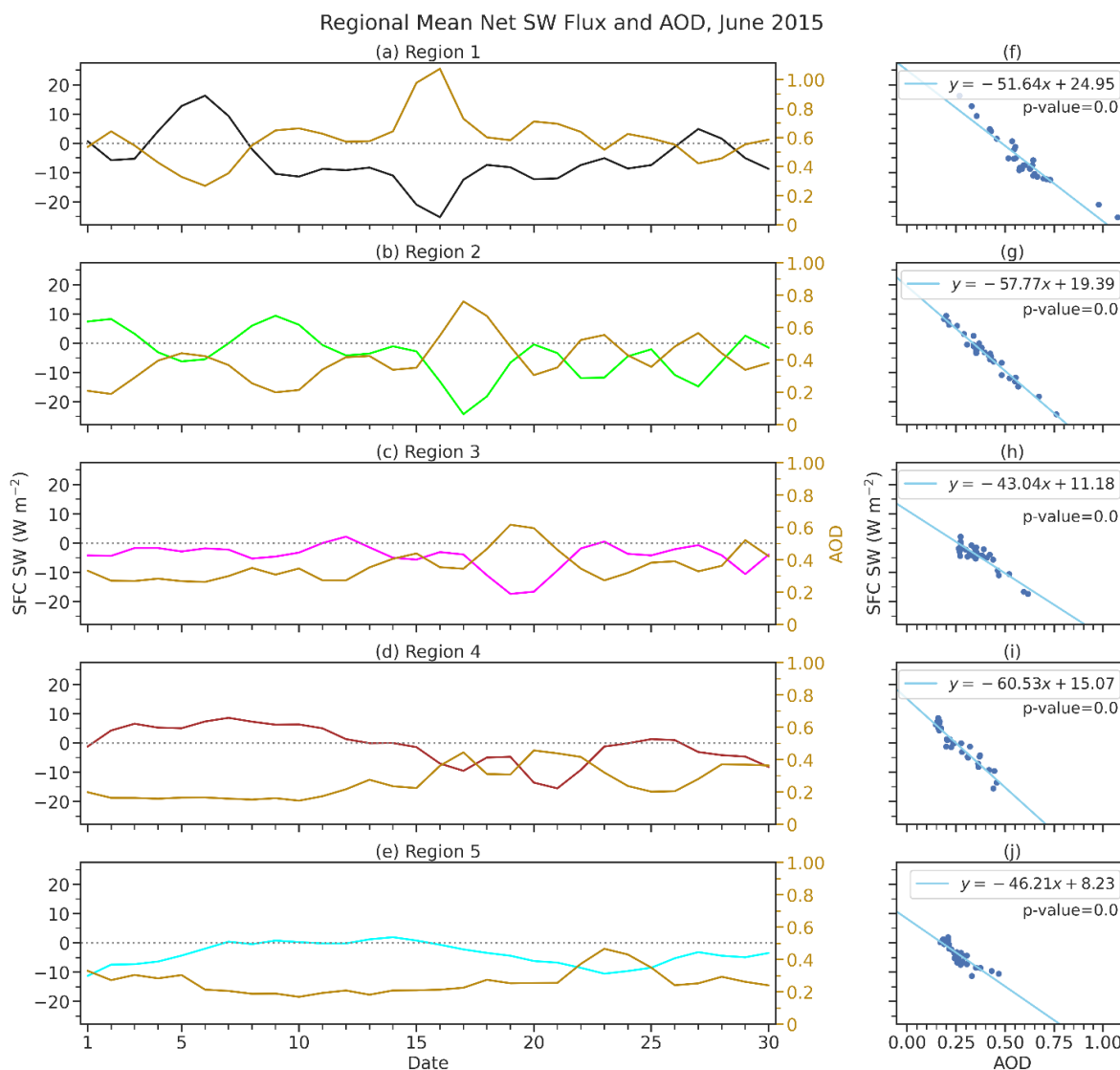
Figure 13. (a)-(e) Anomalies of CERES clear-sky net shortwave flux at the surface (with reference to the 2003-2022 climatology in June; W m^{-2}) over the tropical North Atlantic in Regions 1-5 (see locations in Fig. 12) in June 2015. Black, green, magenta, brown, and cyan lines are regional mean surface net shortwave flux from Regions 1–5. Golden lines show regional mean AOD in Regions 1–5. (f)-(j) Scatterplots of regional mean MODIS AOD versus anomalies of CERES clear-sky surface net shortwave fluxes (W m^{-2}) in Regions 1-5.

Figure 13 tracks the magnitude of surface net SW flux perturbation and its relationship to AOD by calculating regional averages of both variables within three subregions over the tropical North Atlantic (Regions 1–3; Fig. 12a), over the southeastern U.S.

510 (Region 4) and over the tropical eastern Pacific (Region 5). Regions 1– 3 show a steady increase in AOD and a decline in anomalies of surface SW flux as the dust plume propagated westward (Fig. 13a-c). The previously described division of the dust plume resulted in higher regional AOD and lower SW flux in the Pacific (Region 5), while signals are much weaker in the southeastern U.S. due to a higher surface albedo over land (Region 4; Fig. 13d-e). The magnitude of surface SW perturbation is nearly linear with the magnitude of AOD in Regions 1-3 (Fig. 13f-j), about $-43.0 \pm 7.9 \sim -60.5 \pm 7.6$ (95%

515 confidence intervals) W m^{-2} AOD^{-1}, similar to the nearly linear the relationship between increased AOD due to dust and perturbed TOA SW fluxes over the tropical North Atlantic found by previous studies, e.g., $-36.5 \pm 4.8 \sim -49.7 \pm 7.1$ W m^{-2} AOD^{-1} (Song et al. 2018). A similar linear relationship between AOD magnitude and surface net SW flux was found for the 2020 case (Figure S4), with 2020 showing slightly less negative coefficients in Regions 1 and 2, but slightly more negative in Region 3 in comparison with the 2015 event.

520

The anomalies of surface net LW fluxes versus AOD in the June 2015 event are shown in Figure S5. A nearly linear relationship between AOD and net LW fluxes was also found over the tropical North Atlantic (Regions 1-2), but not over the Caribbean Basin (Region 3), likely being interfered with by other factors modifying surface longwave flux, such as low-level moisture content and SST.

525 **4.4.2 Air Quality Impacts**

The air quality impacts of the 2015 trans-Atlantic dust plume seem to be minor in the United States. Figure 14 shows the daily PM$_{2.5}$ concentration and Air Quality Index (AQI) from 20 to 25 June 2015. PM$_{2.5}$ concentrations increased as the dust plume arrived in the Gulf states around 21 June, propagated northward to the central U.S. and southern Midwest states on 23 June, and eventually decayed around 25 June (Figs. 14 b-f). While PM$_{2.5}$ measurements are well within the U.S. Environmental

530 Protection Agency (EPA) standard of 35 µg m^{-3}, some sites over Texas, Oklahoma, Kansas, Louisiana, Mississippi, Alabama, Georgia, Tennessee, and West Virginia show PM$_{2.5}$ concentration exceeded the World Health Organization (WHO) air quality guidelines of 25 µg m^{-3} during the event, with the strongest impacts on 23 June (Fig. 14d). Chen et al. (2018) also found four sites in Texas reporting daily maximum PM$_{2.5}$ concentrations above 36.3 µg m^{-3} during the event.
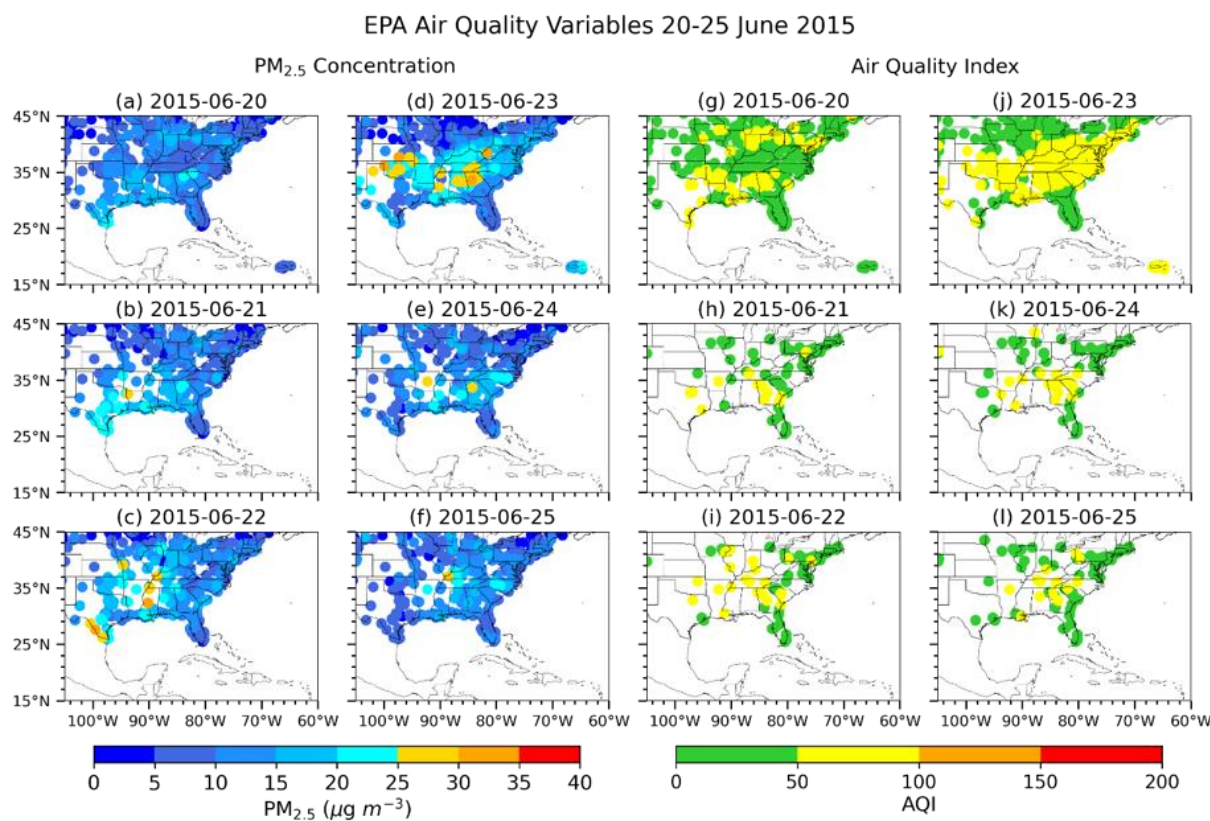
Figure 14. (a)-(f) Daily PM$_{2.5}$ concentrations (μg m^{-3}) and (g)-(l) Air Quality Index (AQI) from EPA Air Quality System (AQS) stations from 20 to 25 June 2015. AQI values of 0–50 indicate good air quality (green), 51–100 for moderate condition (yellow), 101–150 for unhealthy for sensitive groups (orange), and 151–200 for unhealthy condition (red).

AQI gives a similar story with all daily ratings being in the "Good" (green) to "Moderate" (yellow) range (Figs. 14g-l). The relatively weak perturbation of the African dust plume on AQI and PM$_{2.5}$ records in the June 2015 event is associated with the extremely strong CLLJ during 17–25 June that dispersed the part of the plume to the eastern Pacific, which greatly reduced the amount of dust to the continental U.S. This suggests that air quality impacts of African dust in the U.S. are sensitive to local circulations such as the CLLJ, in addition to the amount of transported dust over the tropical North Atlantic.

4.5 Comparison to the 2020 extreme trans-Atlantic dust event

In this section, we further compare the June 2015 event with the extreme "Godzilla" dust event in June 2020. The evolution of both events was quite similar. The extremely high AOD over the tropical North Atlantic was led by a great intensification of the AEJ two to four days ahead of time, while the enhancement of the CLLJ and AOD over the Caribbean Basin was almost concurrent (Fig. S6). Note that in both cases the AEJ increased again after the extreme trans-Atlantic dust events we focused

on, e.g., around 21–23 June 2015 and 24–28 June 2020, consistent with the formation of another trans-Atlantic African dust
plume (Fig. 3 here and Fig. 1 of Pu and Jin 2021).

The peak magnitude of regional mean MODIS AOD in the tropical North Atlantic was lower in 2015 (~0.71) than they were
in 2020 (~1.0; Fig. S6a), consistent with the lower AOD over western North Africa (~0.73 vs. ~1.0) and a weaker AEJ in the
2015 event. The magnitude of AOD over the Caribbean Basin in the 2015 case is also lower than that of 2020 (~0.66 vs.
~0.96), along with a stronger CLLJ in the 2015 event (Fig. S6b) that advected a portion of the dust plume away to the eastern
Pacific, resulting in much weaker air quality impacts in the 2015 event than that of the 2020 event.

In terms of dust emissions, increased surface wind speeds in dust source regions over western North Africa and favorable land
surface conditions, such as soil moisture deficit and vegetation decay in the Sahel, are found in both events. However, the
magnitude and duration of AEE over western North Africa in the 2015 event (0.74, one day) is much weaker than that of the
2020 event (0.90, six days). In fact, the magnitude of African AEE in the 2015 event is slightly below the mean of all the
summertime AEEs during 2003–2022 (~0.76; Fig. 1d). The quite moderate AEE in the dust source regions and the
disproportionally high dust loading over the tropical North Atlantic (i.e., the second strongest AEE following the 2020 event)
suggests the importance of atmospheric circulation conditions that facilitate the westward transport of African dust to the
ocean, i.e., the extremely intensified AEJ (the fourth for 11–16 June, during 1979–2022) and CLLJ (the strongest for 17–22
June, during 1979–2022), along with the westward extension of the NASH.

5 Discussion

Several uncertainties are associated with the analysis of the June 2015 extreme African dust event. We mainly use satellite
retrievals, i.e., MODIS and VIIRS, to examine the magnitude of the event. Since AOD at 550 nm from the polar-orbiting
satellites is only available one time daily, with areas of missing values due to clouds or retrieval uncertainties, the magnitude
of the dust plume may be underestimated as sub-daily variations are not able to be captured. This is also revealed by the
comparison between satellite AOD with AERONET sub-daily AOD during the event (Fig. 4). The daytime maxima recorded
by ground observations were largely missed by MODIS and VIIRS AOD. On the other hand, AERONET records also have
drawbacks such as limited spatial coverage, e.g., very few sites over the central to eastern tropical North Atlantic, thus
combining both datasets provides a better characterization of the event.

We found that the extremely high loading of dust over the tropical North Atlantic is due to a moderate increase of African dust
emissions and strongly enhanced AEJ, NASH, and CLLJ over the tropical North Atlantic and Caribbean Basin that advected
African dust westward. While previous modelling studies show that African dust aerosols can lead to a higher, northward
displaced, and intensified AEJ via their radiative effects (e.g., Wilcox et al. 2010; Reale et al. 2011; Grogan et al. 2017; Bercos-

Hickey et al. 2017, 2020), to what extent the extreme dust plume may affect the circulation patterns and consequently feedback to its westward propagation is not fully clear in our observational study and warrants further examination in the future.

While CERES TOA radiative fluxes are from satellite retrievals, it should be noted that the surface radiative fluxes are from the radiative transfer model and the results of which are sensitive to prescribed aerosol optical properties, assimilated satellite cloud properties and MODIS AOD. Improved understanding of dust optical properties, such as dust mineralogy from global dust source regions made available by the Earth Surface Mineral Dust Source Investigation (EMIT) mission (Green et al. 2020), will greatly reduce uncertainties related to the radiative effects of extreme trans-Atlantic African dust events and will be explored in future studies.

6 Conclusion

This research seeks to improve the current understanding of extreme trans-Atlantic dust storms by examining the causes and impacts of the second strongest summertime trans-Atlantic African dust event from 2003 to 2022. The June 2015 event was characterized by a one-day aerosol extreme event (AEE) over the dust source regions in western North Africa on 13 June and a five-day AEE over the tropical North Atlantic from 15 to 19 June. The enhanced dust emissions over land are associated with the extremely strong surface wind speeds over western North Africa in Mauritania and Mali and soil moisture deficit and vegetation decay in the southern Sahel. The greatly intensified African easterly jet (AEJ) over West Africa and the eastern tropical North Atlantic from 14–19 June transported a large amount of African dust toward the ocean. From the western tropical North Atlantic to the Gulf of Mexico, the westward extension of the North Atlantic subtropical high (NASH) further advected the dust plume westward. The increased meridional height gradient over the Caribbean Basin resulted in an extremely enhanced Caribbean low-level jet (CLLJ) that further transported the dust plume westward. The anomalously strong easterly jet diverted a portion of the dust plume westward to the eastern tropical Pacific, while the anticyclonic flow of the NASH steered the rest of the plume to the southern U.S.

The dense dust plume reduced the regional mean surface net shortwave flux by about 25.3 W m^{-2} (17.3 W m^{-2}) and increased the net surface longwave by about 3.5 W m^{-2} (3.1 W m^{-2}) over the tropical eastern Atlantic (the Caribbean Basin). Over the tropical eastern Pacific (8°N – 16°N, 90°W – 115°W), a reduction of regional mean net surface shortwave flux by 10.5 W m^{-2} and an increase in longwave of 5.6 W m^{-2} are also found as the dust plume was transported to the region by the extremely strong CLLJ. The arrival of the African dust plume increased PM$_{2.5}$ concentrations over the southern U.S. during 21–25 June. The pollution was the strongest on 23 June, when daily PM$_{2.5}$ concentrations at some sites over Texas, Oklahoma, Kansas, Mississippi, Alabama, Georgia, Tennessee, and West Virginia exceeded the guideline of the World Health Organization of 25 µg m^{-3}. However, none of the sites show a daily mean above the EPA guideline of 35 µg m^{-3}. The air quality index (AQI) never exceeded 100 but was elevated to 51-100 or a "moderate" level for many states. The overall air quality impacts are not

particularly dangerous, likely due to the strengthened CLLJ that deflected part of the African dust plume into the Pacific, resulting in a lower dust loading in the southern U.S.

615

Similar to the "Godzilla" dust event in June 2020, i.e., the strongest trans-Atlantic African dust event in JJA since 2003, circulation extremes also played important roles in the formation of the 2015 extreme trans-Atlantic dust event. Although the magnitude and duration of the dust emissions in the 2015 event are much weaker than the 2020 event, i.e., a one-day AEE with a magnitude slightly below the long-term mean of AEEs, the extremely intensified AEJ (the fourth strongest for 11–16

620   June over 1979–2022) and CLLJ (the strongest for 17–22 June over 1979–2022) and the enhanced (geopotential height reached 95th percentile in June over 1979–2022) and westward extended NASH, all facilitate the westward transport of African dust to the ocean, resulting in a disproportionally high (the second strongest) dust loading over the tropical North Atlantic. Understanding the mechanisms and impacts of extreme trans-Atlantic African dust events like those in 2015 and 2020 is crucial for predicting slimier extreme dust events and mitigating their negative effects on weather, climate, air quality, and human

625   health. This analysis reveals the importance of circulation features over the tropical North Atlantic and the Caribbean Basin, like the NASH, AEJ, and CLLJ, in influencing the westward transportation and dispersion of dust plumes and how that changes the impacts of extreme dust events.

Code availability

Analysis codes can be provided upon request from the corresponding authors.

630   **Data availability**

ERA5 hourly and monthly data at single and pressure levels can be downloaded at https://cds.climate.copernicus.eu/#!/home. MERRA-2 DOD can be downloaded from https://disc.gsfc.nasa.gov/datasets?keywords=MERRA-2&page=1. MODIS AOD can be obtained from https://ladsweb.modaps.eosdis.nasa.gov/search/. IMERG sub-hourly precipitation can be downloaded at https://disc.gsfc.nasa.gov/datasets/GPM_3IMERGHH_06/summary. CALIOP lidar can be downloaded from

635   https://asdc.larc.nasa.gov/project/CALIPSO/CAL_LID_L3_Tropospheric_APro_CloudFree-Standard-V4-20_V4-20. CERES radiation fluxes were obtained from the NASA Langley Research Center CERES ordering tool at https://asdc.larc.nasa.gov/project/CERES/CERES_EBAF_Edition4.2. AERONET station data can be acquired at https://aeronet.gsfc.nasa.gov/. EPA air quality data can be found at https://www.epa.gov/outdoor-air-quality-data/download-daily-data, and SEVIRI dust RGB data are available at https://eumetsatspace.atlassian.net/wiki/spaces/EUM/overview.

Author contributions

The study was conceived by BP. BH performed the analysis with guidance and assistance from BP and QJ. BH wrote the paper with input and edits from BP and QJ.

Competing interests

The authors declare no competing interests.

Acknowledgements

We thank David Mechem and Nathaniel Brunsell for their helpful suggestions for this paper. We also thank Jacob Tindan for his assistance with coding in the early stages of the study.

Financial support

This research has been supported by the National Science Foundation (grant no. AGS-2227707).

References

665   Ackerman, S. A., 1997: Remote sensing aerosols using satellite infrared observations. *J. Geophys. Res. Atmospheres*, **102**, 17069–17079, https://doi.org/10.1029/96JD03066.

Adams, A. M., J. M. Prospero, and C. Zhang, 2012: CALIPSO-Derived Three-Dimensional Structure of Aerosol over the Atlantic Basin and Adjacent Continents. *J. Clim.*, **25**, 6862–6879, https://doi.org/10.1175/JCLI-D-11-00672.1.

Agutu, N. O., C. E. Ndehedehe, J. L. Awange, F. Kirimi, and M. Mwaniki, 2021: Understanding uncertainty of model-
670   reanalysis soil moisture within Greater Horn of Africa (1982–2014). *J. Hydrol.*, **603**, 127169, https://doi.org/10.1016/j.jhydrol.2021.127169.

Akpinar-Elci, M., F. E. Martin, J. G. Behr, and R. Diaz, 2015: Saharan dust, climate variability, and asthma in Grenada, the Caribbean. *Int. J. Biometeorol.*, **59**, 1667–1671, https://doi.org/10.1007/s00484-015-0973-2.

Ashpole, I., and R. Washington, 2012: An automated dust detection using SEVIRI: A multiyear climatology of summertime
675   dustiness in the central and western Sahara. *J. Geophys. Res. Atmospheres*, **117**, https://doi.org/10.1029/2011JD016845.

Asutosh, A., V. Vinoj, N. Murukesh, R. Ramisetty, and N. Mittal, 2022: Investigation of June 2020 giant Saharan dust storm using remote sensing observations and model reanalysis. *Sci. Rep.*, **12**, 6114, https://doi.org/10.1038/s41598-022-10017-1.

680   Barkan, J., H. Kutiel, P. Alpert, and P. Kishcha, 2004: Synoptics of dust intrusion days from the African continent into the Atlantic Ocean. *J. Geophys. Res. Atmospheres*, **109**, https://doi.org/10.1029/2003JD004416.

Barkley, A. E., and Coauthors, 2022: Interannual Variability in the Source Location of North African Dust Transported to the Amazon. *Geophys. Res. Lett.*, **49**, e2021GL097344, https://doi.org/10.1029/2021GL097344.

Beck, H. E., and Coauthors, 2021: Evaluation of 18 satellite- and model-based soil moisture products using in situ
685   measurements from 826 sensors. *Hydrol. Earth Syst. Sci.*, **25**, 17–40, https://doi.org/10.5194/hess-25-17-2021.

Bercos-Hickey, E., T. R. Nathan, and S.-H. Chen, 2017: Saharan dust and the African easterly jet–African easterly wave system: Structure, location and energetics. *Q. J. R. Meteorol. Soc.*, **143**, 2797–2808, https://doi.org/10.1002/qj.3128.

——, ——, and ——, 2020: On the Relationship between the African Easterly Jet, Saharan Mineral Dust Aerosols, and West African Precipitation. *J. Clim.*, **33**, 3533–3546, https://doi.org/10.1175/JCLI-D-18-0661.1.

690   Bou Karam, D., E. Williams, M. Janiga, C. Flamant, M. McGraw-Herdeg, J. Cuesta, A. Auby, and C. Thorncroft, 2014: Synoptic-scale dust emissions over the Sahara Desert initiated by a moist convective cold pool in early August 2006. *Q. J. R. Meteorol. Soc.*, **140**, 2591–2607, https://doi.org/10.1002/qj.2326.

Bozlaker, A., J. M. Prospero, J. Price, and S. Chellam, 2019: Identifying and Quantifying the Impacts of Advected North African Dust on the Concentration and Composition of Airborne Fine Particulate Matter in Houston and Galveston,
695   Texas. *J. Geophys. Res. Atmospheres*, **124**, 12282–12300, https://doi.org/10.1029/2019JD030792.

Braun, S. A., 2010: Reevaluating the Role of the Saharan Air Layer in Atlantic Tropical Cyclogenesis and Evolution. *Mon. Weather Rev.*, **138**, 2007–2037, https://doi.org/10.1175/2009MWR3135.1.

Brindley, H., P. Knippertz, C. Ryder, and I. Ashpole, 2012: A critical evaluation of the ability of the Spinning Enhanced Visible and Infrared Imager (SEVIRI) thermal infrared red-green-blue rendering to identify dust events: Theoretical analysis. *J. Geophys. Res. Atmospheres*, **117**, https://doi.org/10.1029/2011JD017326.

Brindley, H. E., and J. E. Russell, 2009: An assessment of Saharan dust loading and the corresponding cloud-free longwave direct radiative effect from geostationary satellite observations. *J. Geophys. Res. Atmospheres*, **114**, https://doi.org/10.1029/2008JD011635.

Bristow, C. S., K. A. Hudson-Edwards, and A. Chappell, 2010: Fertilizing the Amazon and equatorial Atlantic with West African dust. *Geophys. Res. Lett.*, **37**, https://doi.org/10.1029/2010GL043486.

Brocca, L., C. Massari, T. Pellarin, P. Filippucci, L. Ciabatta, S. Camici, Y. H. Kerr, and D. Fernández-Prieto, 2020: River flow prediction in data scarce regions: soil moisture integrated satellite rainfall products outperform rain gauge observations in West Africa. *Sci. Rep.*, **10**, 12517, https://doi.org/10.1038/s41598-020-69343-x.

Buchard, V., and Coauthors, 2017: The MERRA-2 Aerosol Reanalysis, 1980 Onward. Part II: Evaluation and Case Studies. *J. Clim.*, **30**, 6851–6872, https://doi.org/10.1175/JCLI-D-16-0613.1.

Burpee, R. W., 1972: The Origin and Structure of Easterly Waves in the Lower Troposphere of North Africa. *J. Atmospheric Sci.*, **29**, 77–90, https://doi.org/10.1175/1520-0469(1972)029<0077:TOASOE>2.0.CO;2.

Carlson, T. N., and J. M. Prospero, 1972: The Large-Scale Movement of Saharan Air Outbreaks over the Northern Equatorial Atlantic. *J. Appl. Meteorol. Climatol.*, **11**, 283–297, https://doi.org/10.1175/1520-0450(1972)011<0283:TLSMOS>2.0.CO;2.

——, and R. S. Caverly, 1977: Radiative characteristics of Saharan dust at solar wavelengths. *J. Geophys. Res. 1896-1977*, **82**, 3141–3152, https://doi.org/10.1029/JC082i021p03141.

Caton Harrison, T., R. Washington, and S. Engelstaedter, 2021: Satellite-Derived Characteristics of Saharan Cold Pool Outflows During Boreal Summer. *J. Geophys. Res. Atmospheres*, **126**, e2020JD033387, https://doi.org/10.1029/2020JD033387.

Chen, S.-P., C.-H. Lu, J. McQueen, and P. Lee, 2018: Application of satellite observations in conjunction with aerosol reanalysis to characterize long-range transport of African and Asian dust on air quality in the contiguous U.S. *Atmos. Environ.*, **187**, 174–195, https://doi.org/10.1016/j.atmosenv.2018.05.038.

Claquin, T., and Coauthors, 2003: Radiative forcing of climate by ice-age atmospheric dust. *Clim. Dyn.*, **20**, 193–202, https://doi.org/10.1007/s00382-002-0269-1.

Cook, K. H., 1999: Generation of the African Easterly Jet and Its Role in Determining West African Precipitation. *J. Clim.*, **12**, 1165–1184, https://doi.org/10.1175/1520-0442(1999)012<1165:GOTAEJ>2.0.CO;2.

Cowie, S. M., P. Knippertz, and J. H. Marsham, 2014: A climatology of dust emission events from northern Africa using long-term surface observations. *Atmospheric Chem. Phys.*, **14**, 8579–8597, https://doi.org/10.5194/acp-14-8579-2014.

Cowie, S. M., J. H. Marsham, and P. Knippertz, 2015: The importance of rare, high-wind events for dust uplift in northern Africa. *Geophys. Res. Lett.*, **42**, 8208–8215, https://doi.org/10.1002/2015GL065819.

DeMott, P. J., K. Sassen, M. R. Poellot, D. Baumgardner, D. C. Rogers, S. D. Brooks, A. J. Prenni, and S. M. Kreidenweis, 2003: African dust aerosols as atmospheric ice nuclei. *Geophys. Res. Lett.*, **30**, https://doi.org/10.1029/2003GL017410.

735 Didan, K., A. B. Munoz, and A. Huete, MODIS Vegetation Index User's Guide (MOD13 Series).

Doelling, D. R., M. Sun, L. T. Nguyen, M. L. Nordeen, C. O. Haney, D. F. Keyes, and P. E. Mlynczak, 2016: Advances in Geostationary-Derived Longwave Fluxes for the CERES Synoptic (SYN1deg) Product. *J. Atmospheric Ocean. Technol.*, **33**, 503–521, https://doi.org/10.1175/JTECH-D-15-0147.1.

Doherty, O. M., N. Riemer, and S. Hameed, 2008: Saharan mineral dust transport into the Caribbean: Observed atmospheric 740 controls and trends. *J. Geophys. Res. Atmospheres*, **113**, https://doi.org/10.1029/2007JD009171.

Dunion, J. P., 2011: Rewriting the Climatology of the Tropical North Atlantic and Caribbean Sea Atmosphere. *J. Clim.*, **24**, 893–908, https://doi.org/10.1175/2010JCLI3496.1.

——, and C. S. Velden, 2004: The Impact of the Saharan Air Layer on Atlantic Tropical Cyclone Activity. *Bull. Am. Meteorol. Soc.*, **85**, 353–366, https://doi.org/10.1175/BAMS-85-3-353.

745 Engelstaedter, S., and R. Washington, 2007: Atmospheric controls on the annual cycle of North African dust. *J. Geophys. Res. Atmospheres*, **112**, https://doi.org/10.1029/2006JD007195.

——, I. Tegen, and R. Washington, 2006: North African dust emissions and transport. *Earth-Sci. Rev.*, **79**, 73–100, https://doi.org/10.1016/j.earscirev.2006.06.004.

Española, S., M. Urrutia-Pereira, L. Rizzo, P. Staffeld, H. Chong Neto, G. Viegi, and D. Solé, 2021: P U B L I C A T I O N S 750 CODON Allergologia et immunopathologia Dust from the Sahara to the American Continent: Health impacts. *Allergol. Immunopathol. (Madr.)*, **49**, 187–194, https://doi.org/10.15586/aei.v49i4.436.

Evan, A. T., S. Fiedler, C. Zhao, L. Menut, K. Schepanski, C. Flamant, and O. Doherty, 2015: Derivation of an observation-based map of North African dust emission. *Aeolian Res.*, **16**, 153–162, https://doi.org/10.1016/j.aeolia.2015.01.001.

——, C. Flamant, M. Gaetani, and F. Guichard, 2016: The past, present and future of African dust. *Nature*, **531**, 493–495, 755 https://doi.org/10.1038/nature17149.

Evans, S., S. Malyshev, P. Ginoux, and E. Shevliakova, 2019: The Impacts of the Dust Radiative Effect on Vegetation Growth in the Sahel. *Glob. Biogeochem. Cycles*, **33**, 1582–1593, https://doi.org/10.1029/2018GB006128.

Fiedler, S., M. L. Kaplan, and P. Knippertz, 2015: The importance of Harmattan surges for the emission of North African dust aerosol. *Geophys. Res. Lett.*, **42**, 9495–9504, https://doi.org/10.1002/2015GL065925.

760 Foltz, G. R., A. T. Evan, H. P. Freitag, S. Brown, and M. J. McPhaden, 2013: Dust Accumulation Biases in PIRATA Shortwave Radiation Records. *J. Atmospheric Ocean. Technol.*, **30**, 1414–1432, https://doi.org/10.1175/JTECH-D-12-00169.1.

Fontaine, B., N. Philippon, S. Trzaska, and P. Roucou, 2002: Spring to summer changes in the West African monsoon through NCEP/NCAR reanalyses (1968–1998). *J. Geophys. Res. Atmospheres*, **107**, ACL 1-1-ACL 1-9, https://doi.org/10.1029/2001JD000834.

765 Francis, D., R. Fonseca, N. Nelli, J. Cuesta, M. Weston, A. Evan, and M. Temimi, 2020: The Atmospheric Drivers of the Major Saharan Dust Storm in June 2020. *Geophys. Res. Lett.*, **47**, e2020GL090102, https://doi.org/10.1029/2020GL090102.

——, N. Nelli, R. Fonseca, M. Weston, C. Flamant, and C. Cherif, 2022: The dust load and radiative impact associated with the June 2020 historical Saharan dust storm. *Atmos. Environ.*, **268**, 118808,
770 https://doi.org/10.1016/j.atmosenv.2021.118808.

Freitas, E. da S., and Coauthors, 2020: The performance of the IMERG satellite-based product in identifying sub-daily rainfall events and their properties. *J. Hydrol.*, **589**, 125128, https://doi.org/10.1016/j.jhydrol.2020.125128.

Gelaro, R., and Coauthors, 2017: The Modern-Era Retrospective Analysis for Research and Applications, Version 2 (MERRA-2). *J. Clim.*, **30**, 5419–5454, https://doi.org/10.1175/JCLI-D-16-0758.1.

775 Giles, D. M., and Coauthors, 2019: Advancements in the Aerosol Robotic Network (AERONET) Version 3 database – automated near-real-time quality control algorithm with improved cloud screening for Sun photometer aerosol optical depth (AOD) measurements. *Atmospheric Meas. Tech.*, **12**, 169–209, https://doi.org/10.5194/amt-12-169-2019.

Gillette, D. A., J. Adams, A. Endo, D. Smith, and R. Kihl, 1980: Threshold velocities for input of soil particles into the air by desert soils. *J. Geophys. Res. Oceans*, **85**, 5621–5630, https://doi.org/10.1029/JC085iC10p05621.

780 Goudie, A. S., 2014: Desert dust and human health disorders. *Environ. Int.*, **63**, 101–113, https://doi.org/10.1016/j.envint.2013.10.011.

Goudie, A. S., and N. J. Middleton, 2001: Saharan dust storms: nature and consequences. *Earth-Sci. Rev.*, **56**, 179–204, https://doi.org/10.1016/S0012-8252(01)00067-8.

Green, R. O., and Coauthors, 2020: The Earth Surface Mineral Dust Source Investigation: An Earth Science Imaging
785 Spectroscopy Mission. *2020 IEEE Aerospace Conference*, 2020 IEEE Aerospace Conference, 1–15.

Grogan, D. F. P., T. R. Nathan, and S.-H. Chen, 2017: Saharan Dust and the Nonlinear Evolution of the African Easterly Jet–African Easterly Wave System. *J. Atmospheric Sci.*, **74**, 27–47, https://doi.org/10.1175/JAS-D-16-0118.1.

Groß, S., V. Freudenthaler, K. Schepanski, C. Toledano, A. Schäfler, A. Ansmann, and B. Weinzierl, 2015: Optical properties of long-range transported Saharan dust over Barbados as measured by dual-wavelength depolarization Raman lidar
790 measurements. *Atmospheric Chem. Phys.*, **15**, 11067–11080, https://doi.org/10.5194/acp-15-11067-2015.

Gyan, K., W. Henry, S. Lacaille, A. Laloo, C. Lamsee-Ebanks, S. McKay, R. M. Antoine, and M. A. Monteil, 2005: African dust clouds are associated with increased paediatric asthma accident and emergency admissions on the Caribbean island of Trinidad. *Int. J. Biometeorol.*, **49**, 371–376, https://doi.org/10.1007/s00484-005-0257-3.

Haarig, M., and Coauthors, 2017: Triple-wavelength depolarization-ratio profiling of Saharan dust over Barbados during
795 SALTRACE in 2013 and 2014. *Atmospheric Chem. Phys.*, **17**, 10767–10794, https://doi.org/10.5194/acp-17-10767-2017.

Hansell, R. A., and Coauthors, 2010: An Assessment of the Surface Longwave Direct Radiative Effect of Airborne Saharan Dust during the NAMMA Field Campaign. *J. Atmospheric Sci.*, **67**, 1048–1065, https://doi.org/10.1175/2009JAS3257.1.

800   Haywood, J., and Coauthors, 2003: Radiative properties and direct radiative effect of Saharan dust measured by the C-130 aircraft during SHADE: 1. Solar spectrum. *J. Geophys. Res. Atmospheres*, **108**, https://doi.org/10.1029/2002JD002687.

Haywood, J. M., P. N. Francis, M. D. Glew, and J. P. Taylor, 2001: Optical properties and direct radiative effect of Saharan dust: A case study of two Saharan dust outbreaks using aircraft data. *J. Geophys. Res. Atmospheres*, **106**, 18417–
805   18430, https://doi.org/10.1029/2000JD900319.

Helgren, D. M., and J. M. Prospero, 1987: Wind Velocities Associated with Dust Deflation Events in the Western Sahara. *J. Appl. Meteorol. Climatol.*, **26**, 1147–1151, https://doi.org/10.1175/1520-0450(1987)026<1147:WVAWDD>2.0.CO;2.

Hersbach, H., and Coauthors, 2020: The ERA5 global reanalysis. *Q. J. R. Meteorol. Soc.*, **146**, 1999–2049,
810   https://doi.org/10.1002/qj.3803.

Highwood, E. J., J. M. Haywood, M. D. Silverstone, S. M. Newman, and J. P. Taylor, 2003: Radiative properties and direct effect of Saharan dust measured by the C-130 aircraft during Saharan Dust Experiment (SHADE): 2. Terrestrial spectrum. *J. Geophys. Res. Atmospheres*, **108**, https://doi.org/10.1029/2002JD002552.

Holben, B. N., and Coauthors, 1998: AERONET—A Federated Instrument Network and Data Archive for Aerosol
815   Characterization. *Remote Sens. Environ.*, **66**, 1–16, https://doi.org/10.1016/S0034-4257(98)00031-5.

Holben, B. N., and Coauthors, 2001: An emerging ground-based aerosol climatology: Aerosol optical depth from AERONET. *J. Geophys. Res. Atmospheres*, **106**, 12067–12097, https://doi.org/10.1029/2001JD900014.

Hsu, N. C., J. Lee, A. M. Sayer, W. Kim, C. Bettenhausen, and S. -C. Tsay, 2019: VIIRS Deep Blue Aerosol Products Over Land: Extending the EOS Long-Term Aerosol Data Records. *J. Geophys. Res. Atmospheres*, **124**, 4026–4053,
820   https://doi.org/10.1029/2018JD029688.

Huang, J., C. Zhang, and J. M. Prospero, 2010: African dust outbreaks: A satellite perspective of temporal and spatial variability over the tropical Atlantic Ocean. *J. Geophys. Res. Atmospheres*, **115**, https://doi.org/10.1029/2009JD012516.

Huneeus, N., and Coauthors, 2011: Global dust model intercomparison in AeroCom phase I. *Atmospheric Chem. Phys.*, **11**,
825   7781–7816, https://doi.org/10.5194/acp-11-7781-2011.

Jenkins, G. S., and A. Pratt, 2008: Saharan dust, lightning and tropical cyclones in the eastern tropical Atlantic during NAMMA-06. *Geophys. Res. Lett.*, **35**, https://doi.org/10.1029/2008GL033979.

——, A. S. Pratt, and A. Heymsfield, 2008: Possible linkages between Saharan dust and tropical cyclone rain band invigoration in the eastern Atlantic during NAMMA-06. *Geophys. Res. Lett.*, **35**, https://doi.org/10.1029/2008GL034072.

830   Jickells, T. D., S. Dorling, W. G. Deuser, T. M. Church, R. Arimoto, and J. M. Prospero, 1998: Air-borne dust fluxes to a deep water sediment trap in the Sargasso Sea. *Glob. Biogeochem. Cycles*, **12**, 311–320, https://doi.org/10.1029/97GB03368.

——, A. R. Baker, and R. Chance, 2016: Atmospheric transport of trace elements and nutrients to the oceans. *Philos. Trans. R. Soc. Math. Phys. Eng. Sci.*, **374**, 20150286, https://doi.org/10.1098/rsta.2015.0286.

835 Johnson, G. C., J. M. Lyman, and N. G. Loeb, 2016: Improving estimates of Earth's energy imbalance. *Nat. Clim. Change*, **6**, 639–640, https://doi.org/10.1038/nclimate3043.

Jones, C., N. Mahowald, and C. Luo, 2003: The role of easterly waves on African desert dust transport. *J. Clim.*, **16**, 3617–3628, https://doi.org/10.1175/1520-0442(2003)016<3617:TROEWO>2.0.CO;2.

Kalashnikova, O. V., and R. A. Kahn, 2008: Mineral dust plume evolution over the Atlantic from MISR and MODIS aerosol
840 retrievals. *J. Geophys. Res. Atmospheres*, **113**, https://doi.org/10.1029/2008JD010083.

Kanitz, T., R. Engelmann, B. Heinold, H. Baars, A. Skupin, and A. Ansmann, 2014: Tracking the Saharan Air Layer with shipborne lidar across the tropical Atlantic. *Geophys. Res. Lett.*, **41**, 1044–1050, https://doi.org/10.1002/2013GL058780.

Karyampudi, V. M., and T. N. Carlson, 1988: Analysis and Numerical Simulations of the Saharan Air Layer and Its Effect on
845 Easterly Wave Disturbances. *J. Atmospheric Sci.*, **45**, 3102–3136, https://doi.org/10.1175/1520-0469(1988)045<3102:AANSOT>2.0.CO;2.

Kato, S., and Coauthors, 2018: Surface Irradiances of Edition 4.0 Clouds and the Earth's Radiant Energy System (CERES) Energy Balanced and Filled (EBAF) Data Product. *J. Clim.*, **31**, 4501–4527, https://doi.org/10.1175/JCLI-D-17-0523.1.

850 Kaufman, Y. J., I. Koren, L. A. Remer, D. Tanré, P. Ginoux, and S. Fan, 2005: Dust transport and deposition observed from the Terra-Moderate Resolution Imaging Spectroradiometer (MODIS) spacecraft over the Atlantic Ocean. *J. Geophys. Res. Atmospheres*, **110**, https://doi.org/10.1029/2003JD004436.

Kim, D., M. Chin, L. A. Remer, T. Diehl, H. Bian, H. Yu, M. E. Brown, and W. R. Stockwell, 2017: Role of surface wind and vegetation cover in multi-decadal variations of dust emission in the Sahara and Sahel. *Atmos. Environ.*, **148**, 282–
855 296, https://doi.org/10.1016/j.atmosenv.2016.10.051.

Kim, M.-H., and Coauthors, 2018: The CALIPSO version 4 automated aerosol classification and lidar ratio selection algorithm. *Atmospheric Meas. Tech.*, **11**, 6107–6135, https://doi.org/10.5194/amt-11-6107-2018.

Knippertz, P., and A. H. Fink, 2006: Synoptic and dynamic aspects of an extreme springtime Saharan dust outbreak. *Q. J. R. Meteorol. Soc.*, **132**, 1153–1177, https://doi.org/10.1256/qj.05.109.

860 ——, and M. C. Todd, 2010: The central west Saharan dust hot spot and its relation to African easterly waves and extratropical disturbances. *J. Geophys. Res. Atmospheres*, **115**, https://doi.org/10.1029/2009JD012819.

——, and ——, 2012: Mineral dust aerosols over the Sahara: Meteorological controls on emission and transport and implications for modeling. *Rev. Geophys.*, **50**, https://doi.org/10.1029/2011RG000362.

Kok, J. F., and Coauthors, 2017: Smaller desert dust cooling effect estimated from analysis of dust size and abundance. *Nat.*
865 *Geosci.*, **10**, 274–278, https://doi.org/10.1038/ngeo2912.

——, and Coauthors, 2021: Contribution of the world's main dust source regions to the global cycle of desert dust. *Atmospheric Chem. Phys.*, **21**, 8169–8193, https://doi.org/10.5194/acp-21-8169-2021.

——, T. Storelvmo, V. A. Karydis, A. A. Adebiyi, N. M. Mahowald, A. T. Evan, C. He, and D. M. Leung, 2023: Mineral dust aerosol impacts on global climate and climate change. *Nat. Rev. Earth Environ.*, **4**, 71–86,
870 https://doi.org/10.1038/s43017-022-00379-5.

Kumar, A., W. Abouchami, S. J. G. Galer, V. H. Garrison, E. Williams, and M. O. Andreae, 2014: A radiogenic isotope tracer study of transatlantic dust transport from Africa to the Caribbean. *Atmos. Environ.*, **82**, 130–143, https://doi.org/10.1016/j.atmosenv.2013.10.021.

Lensky, I. M., and D. Rosenfeld, 2008: Clouds-Aerosols-Precipitation Satellite Analysis Tool (CAPSAT). *Atmospheric Chem. Phys.*, **8**, 6739–6753, https://doi.org/10.5194/acp-8-6739-2008.

Leroux, S., and N. M. J. Hall, 2009: On the Relationship between African Easterly Waves and the African Easterly Jet. *J. Atmospheric Sci.*, **66**, 2303–2316, https://doi.org/10.1175/2009JAS2988.1.

Levin, Z., E. Ganor, and V. Gladstein, 1996: The Effects of Desert Particles Coated with Sulfate on Rain Formation in the Eastern Mediterranean. *J. Appl. Meteorol. Climatol.*, **35**, 1511–1523, https://doi.org/10.1175/1520-0450(1996)035<1511:TEODPC>2.0.CO;2.

Li, F., A. M. Vogelmann, and V. Ramanathan, 2004: Saharan Dust Aerosol Radiative Forcing Measured from Space. *J. Clim.*, **17**, 2558–2571, https://doi.org/10.1175/1520-0442(2004)017<2558:SDARFM>2.0.CO;2.

Li, F., P. Ginoux, and V. Ramaswamy, 2010: Transport of Patagonian dust to Antarctica. *J. Geophys. Res. Atmospheres*, **115**, https://doi.org/10.1029/2009JD012356.

Li, J., E. Garshick, S. Huang, and P. Koutrakis, 2021a: Impacts of El Niño-Southern Oscillation on surface dust levels across the world during 1982–2019. *Sci. Total Environ.*, **769**, 144566, https://doi.org/10.1016/j.scitotenv.2020.144566.

Li, W., L. Li, R. Fu, Y. Deng, and H. Wang, 2011: Changes to the North Atlantic Subtropical High and Its Role in the Intensification of Summer Rainfall Variability in the Southeastern United States. *J. Clim.*, **24**, 1499–1506, https://doi.org/10.1175/2010JCLI3829.1.

Li, Y., J. T. Randerson, N. M. Mahowald, and P. J. Lawrence, 2021b: Deforestation Strengthens Atmospheric Transport of Mineral Dust and Phosphorus from North Africa to the Amazon. *J. Clim.*, **34**, 6087–6096, https://doi.org/10.1175/JCLI-D-20-0786.1.

Liu, H., L. A. Remer, J. Huang, H.-C. Huang, S. Kondragunta, I. Laszlo, M. Oo, and J. M. Jackson, 2014: Preliminary evaluation of S-NPP VIIRS aerosol optical thickness. *J. Geophys. Res. Atmospheres*, **119**, 3942–3962, https://doi.org/10.1002/2013JD020360.

Loeb, N. G., and Coauthors, 2018: Clouds and the Earth's Radiant Energy System (CERES) Energy Balanced and Filled (EBAF) Top-of-Atmosphere (TOA) Edition-4.0 Data Product. *J. Clim.*, **31**, 895–918, https://doi.org/10.1175/JCLI-D-17-0208.1.

Mahowald, N., S. Albani, J. F. Kok, S. Engelstaeder, R. Scanza, D. S. Ward, and M. G. Flanner, 2014: The size distribution of desert dust aerosols and its impact on the Earth system. *Aeolian Res.*, **15**, 53–71, https://doi.org/10.1016/j.aeolia.2013.09.002.

Marsham, J. H., D. J. Parker, C. M. Grams, C. M. Taylor, and J. M. Haywood, 2008: Uplift of Saharan dust south of the intertropical discontinuity. *J. Geophys. Res. Atmospheres*, **113**, https://doi.org/10.1029/2008JD009844.

Martin, E. R., and C. Schumacher, 2011: The Caribbean Low-Level Jet and Its Relationship with Precipitation in IPCC AR4 Models. *J. Clim.*, **24**, 5935–5950, https://doi.org/10.1175/JCLI-D-11-00134.1.

Martínez, M. A., J. Ruiz, and E. Cuevas, 2009: Use of SEVIRI images and derived products in a WMO Sand and dust Storm Warning System. *IOP Conf. Ser. Earth Environ. Sci.*, **7**, 012004, https://doi.org/10.1088/1755-1307/7/1/012004.

Mehra, M., and Coauthors, 2023: Atmospheric heating in the US from saharan dust: Tracking the June 2020 event with surface and satellite observations. *Atmos. Environ.*, **310**, 119988, https://doi.org/10.1016/j.atmosenv.2023.119988.

910   Meloni, D., A. di Sarra, T. Di Iorio, and G. Fiocco, 2005: Influence of the vertical profile of Saharan dust on the visible direct radiative forcing. *J. Quant. Spectrosc. Radiat. Transf.*, **93**, 397–413, https://doi.org/10.1016/j.jqsrt.2004.08.035.

Moulin, C., and I. Chiapello, 2004: Evidence of the control of summer atmospheric transport of African dust over the Atlantic by Sahel sources from TOMS satellites (1979–2000). *Geophys. Res. Lett.*, **31**, https://doi.org/10.1029/2003GL018931.

915   Moulin, C., C. E. Lambert, F. Dulac, and U. Dayan, 1997: Control of atmospheric export of dust from North Africa by the North Atlantic Oscillation. *Nature*, **387**, 691–694, https://doi.org/10.1038/42679.

Muñoz-Sabater, J., and Coauthors, 2021: ERA5-Land: a state-of-the-art global reanalysis dataset for land applications. *Earth Syst. Sci. Data*, **13**, 4349–4383, https://doi.org/10.5194/essd-13-4349-2021.

Myhre, G., A. Grini, J. M. Haywood, F. Stordal, B. Chatenet, D. Tanré, J. K. Sundet, and I. S. A. Isaksen, 2003: Modeling the
920   radiative impact of mineral dust during the Saharan Dust Experiment (SHADE) campaign. *J. Geophys. Res. Atmospheres*, **108**, https://doi.org/10.1029/2002JD002566.

Okin, G. S., N. Mahowald, O. A. Chadwick, and P. Artaxo, 2004: Impact of desert dust on the biogeochemistry of phosphorus in terrestrial ecosystems. *Glob. Biogeochem. Cycles*, **18**, https://doi.org/10.1029/2003GB002145.

Ott, S.-T., A. Ott, D. W. Martin, and J. A. Young, 1991: Analysis of a Trans-Atlantic Saharan Dust Outbreak Based on Satellite
925   and GATE Data. *Mon. Weather Rev.*, **119**, 1832–1850, https://doi.org/10.1175/1520-0493(1991)119<1832:AOATAS>2.0.CO;2.

Pan, W., L. Wu, and C.-L. Shie, 2011: Influence of the Saharan Air Layer on Atlantic tropical cyclone formation during the period 1–12 September 2003. *Adv. Atmospheric Sci.*, **28**, 16–32, https://doi.org/10.1007/s00376-010-9165-5.

Petit, R. H., M. Legrand, I. Jankowiak, J. Molinié, C. Asselin de Beauville, G. Marion, and J. L. Mansot, 2005: Transport of
930   Saharan dust over the Caribbean Islands: Study of an event. *J. Geophys. Res. Atmospheres*, **110**, https://doi.org/10.1029/2004JD004748.

Peyridieu, S., A. Chédin, D. Tanré, V. Capelle, C. Pierangelo, N. Lamquin, and R. Armante, 2010: Saharan dust infrared optical depth and altitude retrieved from AIRS: a focus over North Atlantic – comparison to MODIS and CALIPSO. *Atmospheric Chem. Phys.*, **10**, 1953–1967, https://doi.org/10.5194/acp-10-1953-2010.

935   Piles, M., J. Ballabrera-Poy, and J. Muñoz-Sabater, 2019: Dominant Features of Global Surface Soil Moisture Variability Observed by the SMOS Satellite. *Remote Sens.*, **11**, 95, https://doi.org/10.3390/rs11010095.

Prenni, A. J., M. D. Petters, A. Faulhaber, C. M. Carrico, P. J. Ziemann, S. M. Kreidenweis, and P. J. DeMott, 2009: Heterogeneous ice nucleation measurements of secondary organic aerosol generated from ozonolysis of alkenes. *Geophys. Res. Lett.*, **36**, https://doi.org/10.1029/2008GL036957.

940 Prospero, J. M., 1999: Long-term measurements of the transport of African mineral dust to the southeastern United States: Implications for regional air quality. *J. Geophys. Res. Atmospheres*, **104**, 15917–15927, https://doi.org/10.1029/1999JD900072.

——, and T. N. Carlson, 1970: Radon-222 in the North Atlantic Trade Winds: Its Relationship to Dust Transport from Africa. *Science*, **167**, 974–977, https://doi.org/10.1126/science.167.3920.974.

945 ——, and ——, 1972: Vertical and areal distribution of Saharan dust over the western equatorial north Atlantic Ocean. *J. Geophys. Res. 1896-1977*, **77**, 5255–5265, https://doi.org/10.1029/JC077i027p05255.

——, and ——, 1981: Saharan air outbreaks over the tropical North Atlantic. *Pure Appl. Geophys. PAGEOPH*, **119**, 677–691, https://doi.org/10.1007/BF00878167.

——, and P. J. Lamb, 2003: African Droughts and Dust Transport to the Caribbean: Climate Change Implications. *Science*, 950 **302**, 1024–1027, https://doi.org/10.1126/science.1089915.

——, E. Bonatti, C. Schubert, and T. N. Carlson, 1970: Dust in the Caribbean atmosphere traced to an African dust storm. *Earth Planet. Sci. Lett.*, **9**, 287–293, https://doi.org/10.1016/0012-821X(70)90039-7.

——, P. Ginoux, O. Torres, S. E. Nicholson, and T. E. Gill, 2002: Environmental Characterization of Global Sources of Atmospheric Soil Dust Identified with the Nimbus 7 Total Ozone Mapping Spectrometer (toms) Absorbing Aerosol 955 Product. *Rev. Geophys.*, **40**, 2-1-2–31, https://doi.org/10.1029/2000RG000095.

——, E. Blades, G. Mathison, and R. Naidu, 2005: Interhemispheric transport of viable fungi and bacteria from Africa to the Caribbean with soil dust. *Aerobiologia*, **21**, 1–19, https://doi.org/10.1007/s10453-004-5872-7.

——, A. C. Delany, A. C. Delany, and T. N. Carlson, 2021: The Discovery of African Dust Transport to the Western Hemisphere and the Saharan Air Layer: A History. *Bull. Am. Meteorol. Soc.*, **102**, E1239–E1260, 960 https://doi.org/10.1175/BAMS-D-19-0309.1.

Pu, B., and P. Ginoux, 2018a: Climatic factors contributing to long-term variations in surface fine dust concentration in the United States. *Atmospheric Chem. Phys.*, **18**, 4201–4215, https://doi.org/10.5194/acp-18-4201-2018.

——, and ——, 2018b: How reliable are CMIP5 models in simulating dust optical depth? *Atmospheric Chem. Phys.*, **18**, 12491–12510, https://doi.org/10.5194/acp-18-12491-2018.

965 ——, and Q. Jin, 2021: A Record-Breaking Trans-Atlantic African Dust Plume Associated with Atmospheric Circulation Extremes in June 2020. *Bull. Am. Meteorol. Soc.*, **102**, E1340–E1356, https://doi.org/10.1175/BAMS-D-21-0014.1.

——, and Coauthors, 2020: Retrieving the global distribution of the threshold of wind erosion from satellite data and implementing it into the Geophysical Fluid Dynamics Laboratory land–atmosphere model (GFDL AM4.0/LM4.0). *Atmospheric Chem. Phys.*, **20**, 55–81, https://doi.org/10.5194/acp-20-55-2020.

970 Randles, C. A., and Coauthors, 2017: The MERRA-2 Aerosol Reanalysis, 1980 Onward. Part I: System Description and Data Assimilation Evaluation. *J. Clim.*, **30**, 6823–6850, https://doi.org/10.1175/JCLI-D-16-0609.1.

Reale, O., K. M. Lau, and A. da Silva, 2011: Impact of Interactive Aerosol on the African Easterly Jet in the NASA GEOS-5 Global Forecasting System. *Weather Forecast.*, **26**, 504–519, https://doi.org/10.1175/WAF-D-10-05025.1.

975 Reddy, K., D. V. P. Kumar, Y. N. Ahammed, and M. Naja, 2013: Aerosol vertical profiles strongly affect their radiative forcing uncertainties: study by using ground-based lidar and other measurements. *Remote Sens. Lett.*, **4**, 1018–1027, https://doi.org/10.1080/2150704X.2013.828182.

Roberts, A. J., M. J. Woodage, J. H. Marsham, E. J. Highwood, C. L. Ryder, W. McGinty, S. Wilson, and J. Crook, 2018: Can explicit convection improve modelled dust in summertime West Africa? *Atmospheric Chem. Phys.*, **18**, 9025–9048, https://doi.org/10.5194/acp-18-9025-2018.

980 Rosenfeld, D., Y. Rudich, and R. Lahav, 2001: Desert dust suppressing precipitation: A possible desertification feedback loop. *Proc. Natl. Acad. Sci.*, **98**, 5975–5980, https://doi.org/10.1073/pnas.101122798.

Rutan, D. A., S. Kato, D. R. Doelling, F. G. Rose, L. T. Nguyen, T. E. Caldwell, and N. G. Loeb, 2015: CERES Synoptic Product: Methodology and Validation of Surface Radiant Flux. *J. Atmospheric Ocean. Technol.*, **32**, 1121–1143, https://doi.org/10.1175/JTECH-D-14-00165.1.

985 Sassen, K., 1991: The Polarization Lidar Technique for Cloud Research: A Review and Current Assessment. *Bull. Am. Meteorol. Soc.*, **72**, 1848–1866, https://doi.org/10.1175/1520-0477(1991)072<1848:TPLTFC>2.0.CO;2.

Sayer, A. M., N. C. Hsu, J. Lee, W. V. Kim, and S. T. Dutcher, 2019: Validation, Stability, and Consistency of MODIS Collection 6.1 and VIIRS Version 1 Deep Blue Aerosol Data Over Land. *J. Geophys. Res. Atmospheres*, **124**, 4658–4688, https://doi.org/10.1029/2018JD029598.

990 Schepanski, K., 2018: Transport of Mineral Dust and Its Impact on Climate. *Geosciences*, **8**, 151, https://doi.org/10.3390/geosciences8050151.

Schepanski, K., I. Tegen, B. Laurent, B. Heinold, and A. Macke, 2007: A new Saharan dust source activation frequency map derived from MSG-SEVIRI IR-channels. *Geophys. Res. Lett.*, **34**, https://doi.org/10.1029/2007GL030168.

Schepanski, K., B. Heinold, and I. Tegen, 2017: Harmattan, Saharan heat low, and West African monsoon circulation:
995 modulations on the Saharan dust outflow towards the North Atlantic. *Atmospheric Chem. Phys.*, **17**, 10223–10243, https://doi.org/10.5194/acp-17-10223-2017.

Schmetz, J., P. Pili, S. Tjemkes, D. Just, J. Kerkmann, S. Rota, and A. Ratier, 2002: AN INTRODUCTION TO METEOSAT SECOND GENERATION (MSG). *Bull. Am. Meteorol. Soc.*, **83**, 977–992, https://doi.org/10.1175/1520-0477(2002)083<0977:AITMSG>2.3.CO;2.

1000 Scott, S. R., J. P. Dunion, M. L. Olson, and D. A. Gay, 2022: Lead Isotopes in North American Precipitation Record the Presence of Saharan Dust. *Bull. Am. Meteorol. Soc.*, **103**, E281–E292, https://doi.org/10.1175/BAMS-D-20-0212.1.

Shinn, E. A., D. W. Griffin, and D. B. Seba, 2003: Atmospheric Transport of Mold Spores in Clouds of Desert Dust. *Arch. Environ. Health*, **58**, 498–504.

Slingo, A., and Coauthors, 2006: Observations of the impact of a major Saharan dust storm on the atmospheric radiation
1005 balance. *Geophys. Res. Lett.*, **33**, https://doi.org/10.1029/2006GL027869.

Song, Q., Z. Zhang, H. Yu, S. Kato, P. Yang, P. Colarco, L. A. Remer, and C. L. Ryder, 2018: Net radiative effects of dust in the tropical North Atlantic based on integrated satellite observations and in situ measurements. *Atmospheric Chem. Phys.*, **18**, 11303–11322, https://doi.org/10.5194/acp-18-11303-2018.

Strong, J. D. O., G. A. Vecchi, and P. Ginoux, 2018: The Climatological Effect of Saharan Dust on Global Tropical Cyclones in a Fully Coupled GCM. *J. Geophys. Res. Atmospheres*, **123**, 5538–5559, https://doi.org/10.1029/2017JD027808.

Tegen, I., and A. A. Lacis, 1996: Modeling of particle size distribution and its influence on the radiative properties of mineral dust aerosol. *J. Geophys. Res. Atmospheres*, **101**, 19237–19244, https://doi.org/10.1029/95JD03610.

——, ——, and I. Fung, 1996: The influence on climate forcing of mineral aerosols from disturbed soils. *Nature*, **380**, 419–422, https://doi.org/10.1038/380419a0.

——, E. Bierwirth, B. Heinold, J. Helmert, and M. Wendisch, 2010: Effect of measured surface albedo on modeled Saharan dust solar radiative forcing. *J. Geophys. Res. Atmospheres*, **115**, https://doi.org/10.1029/2009JD013764.

Tindan, J. Z., Q. Jin, and B. Pu, 2023: Understanding day–night differences in dust aerosols over the dust belt of North Africa, the Middle East, and Asia. *Atmospheric Chem. Phys.*, **23**, 5435–5466, https://doi.org/10.5194/acp-23-5435-2023.

Villar-Argaiz, M., M. J. Cabrerizo, J. M. González-Olalla, M. S. Valiñas, S. Rajic, and P. Carrillo, 2018: Growth impacts of Saharan dust, mineral nutrients, and CO2 on a planktonic herbivore in southern Mediterranean lakes. *Sci. Total Environ.*, **639**, 118–128, https://doi.org/10.1016/j.scitotenv.2018.05.041.

Vuolo, M. R., H. Chepfer, L. Menut, and G. Cesana, 2009: Comparison of mineral dust layers vertical structures modeled with CHIMERE-DUST and observed with the CALIOP lidar. *J. Geophys. Res. Atmospheres*, **114**, https://doi.org/10.1029/2008JD011219.

Wang, C., 2007: Variability of the Caribbean Low-Level Jet and its relations to climate. *Clim. Dyn.*, **29**, 411–422, https://doi.org/10.1007/s00382-007-0243-z.

——, S. Dong, A. T. Evan, G. R. Foltz, and S.-K. Lee, 2012: Multidecadal Covariability of North Atlantic Sea Surface Temperature, African Dust, Sahel Rainfall, and Atlantic Hurricanes. *J. Clim.*, **25**, 5404–5415, https://doi.org/10.1175/JCLI-D-11-00413.1.

Wang, J., W. A. Petersen, and D. B. Wolff, 2021: Validation of Satellite-Based Precipitation Products from TRMM to GPM. *Remote Sens.*, **13**, 1745, https://doi.org/10.3390/rs13091745.

Wang, Z., R. Zhong, C. Lai, and J. Chen, 2017: Evaluation of the GPM IMERG satellite-based precipitation products and the hydrological utility. *Atmospheric Res.*, **196**, 151–163, https://doi.org/10.1016/j.atmosres.2017.06.020.

Waters, S. M., S. K. Purdue, R. Armstrong, and Y. Detrés, 2020: Metagenomic investigation of African dust events in the Caribbean. *FEMS Microbiol. Lett.*, **367**, fnaa051, https://doi.org/10.1093/femsle/fnaa051.

Weinzierl, B., and Coauthors, 2017: The Saharan Aerosol Long-Range Transport and Aerosol–Cloud-Interaction Experiment: Overview and Selected Highlights. *Bull. Am. Meteorol. Soc.*, **98**, 1427–1451, https://doi.org/10.1175/BAMS-D-15-00142.1.

Wielicki, B. A., B. R. Barkstrom, E. F. Harrison, R. B. Lee, G. L. Smith, and J. E. Cooper, 1996: Clouds and the Earth's Radiant Energy System (CERES): An Earth Observing System Experiment. *Bull. Am. Meteorol. Soc.*, **77**, 853–868, https://doi.org/10.1175/1520-0477(1996)077<0853:CATERE>2.0.CO;2.

Wilcox, E. M., K. M. Lau, and K.-M. Kim, 2010: A northward shift of the North Atlantic Ocean Intertropical Convergence Zone in response to summertime Saharan dust outbreaks. *Geophys. Res. Lett.*, **37**, https://doi.org/10.1029/2009GL041774.

1045 Winker, D. M., W. H. Hunt, and M. J. McGill, 2007: Initial performance assessment of CALIOP. *Geophys. Res. Lett.*, **34**, https://doi.org/10.1029/2007GL030135.

Wu, C., Z. Lin, and X. Liu, 2020: The global dust cycle and uncertainty in CMIP5 (Coupled Model Intercomparison Project phase 5) models. *Atmospheric Chem. Phys.*, **20**, 10401–10425, https://doi.org/10.5194/acp-20-10401-2020.

Xu, H., and Coauthors, 2017: Warming effect of dust aerosols modulated by overlapping clouds below. *Atmos. Environ.*, **166**,
1050   393–402, https://doi.org/10.1016/j.atmosenv.2017.07.036.

Yin, Y., S. Wurzler, Z. Levin, and T. G. Reisin, 2002: Interactions of mineral dust particles and clouds: Effects on precipitation and cloud optical properties. *J. Geophys. Res. Atmospheres*, **107**, AAC 19-14, https://doi.org/10.1029/2001JD001544.

Yin, Z.-Y., A. Maytubby, and X. Liu, 2022: Variation Patterns of the ENSO's Effects on Dust Activity in North Africa, Arabian Peninsula, and Central Asia of the Dust Belt. *Climate*, **10**, 150, https://doi.org/10.3390/cli10100150.

1055 Yorks, J. E., M. McGill, S. Rodier, M. Vaughan, Y. Hu, and D. Hlavka, 2009: Radiative effects of African dust and smoke observed from Clouds and the Earth's Radiant Energy System (CERES) and Cloud-Aerosol Lidar with Orthogonal Polarization (CALIOP) data. *J. Geophys. Res.-Atmospheres*, **114**, D00H04, https://doi.org/10.1029/2009JD012000.

Yu, H., and Coauthors, 2006: A review of measurement-based assessments of the aerosol direct radiative effect and forcing. *Atmospheric Chem. Phys.*, **6**, 613–666, https://doi.org/10.5194/acp-6-613-2006.

1060 Yu, H., and Coauthors, 2015a: The fertilizing role of African dust in the Amazon rainforest: A first multiyear assessment based on data from Cloud-Aerosol Lidar and Infrared Pathfinder Satellite Observations. *Geophys. Res. Lett.*, **42**, 1984–1991, https://doi.org/10.1002/2015GL063040.

——, and Coauthors, 2015b: Quantification of trans-Atlantic dust transport from seven-year (2007–2013) record of CALIPSO lidar measurements. *Remote Sens. Environ.*, **159**, 232–249, https://doi.org/10.1016/j.rse.2014.12.010.

1065 ——, and Coauthors, 2019: Estimates of African Dust Deposition Along the Trans-Atlantic Transit Using the Decadelong Record of Aerosol Measurements from CALIOP, MODIS, MISR, and IASI. *J. Geophys. Res. Atmospheres*, **124**, 7975–7996, https://doi.org/10.1029/2019JD030574.

——, and Coauthors, 2021: Observation and modeling of the historic "Godzilla" African dust intrusion into the Caribbean Basin and the southern US in June 2020. *Atmospheric Chem. Phys.*, **21**, 12359–12383, https://doi.org/10.5194/acp-
1070   21-12359-2021.